Aperiodic rhythms of the inferior olive

Pascal Warnaar[1,3], Mario Negrello[1,3,4], Vincenzo Romano[1], Cullen B. Owens[1], Sander Lindeman[1], Elisabetta Iavarone[1], Jochen K. Spanke[1], Laurens W.J. Bosman[1]

and Chris I. De Zeeuw[1,2,4]

[1] Department of Neuroscience, Erasmus MC, Rotterdam, the Netherlands

[2] Netherlands Institute for Neuroscience, Royal Academy of Arts and Sciences, Amsterdam, the Netherlands

[3] These authors contributed equally

[4] Correspondence to: M. Negrello, Department of Neuroscience, Erasmus MC, PO Box 2040, 3000 CA Rotterdam, the Netherlands, m.negrello@erasmusmc.nl or C.I. De Zeeuw, Department of Neuroscience, Erasmus MC, PO Box 2040, 3000 CA Rotterdam, the Netherlands, c.dezeeuw@erasmusmc.nl

1

ABSTRACT

Inferior olivary activity causes both short-term and long-term changes in cerebellar output underlying motor adaptation and motor learning, respectively. Many of its neurons engage in coherent subthreshold oscillations and are extensively coupled via gap junctions. Studies in reduced preparations suggest that these properties promote rhythmic, synchronized output. However, how these properties interact with synaptic inputs controlling inferior olivary output in intact, awake behaving animals is poorly understood. Here we combine electrophysiological recordings in awake mice with a novel and realistic tissue-scale computational model of the inferior olive to study the relative impact of intrinsic and extrinsic mechanisms governing its activity. Our data and model suggest that oscillations are present in the awake state, but that the period of subthreshold oscillations is variable, resulting in semi-periodic activity, which result in the high unpredictability of sensory-triggered complex spikes occurring in windows of opportunity lasting a few tens of milliseconds. To test the resonant properties of complex spike firing we used different temporal patterns of sensory stimulation in awake mice. Resonance was found to be limited to short intervals no more than a few hundred milliseconds, which could be explained by our network model to be a result of synaptic input to the inferior olive. The model also shows how gap junctional coupling stiffens the olivary network response to sensory modulation of complex spike rhythmicity. Interactions between intrinsic properties and extrinsic inputs can explain short-lasting semi-periodic variations of the spiking rhythms of olivary neurons even though their long-term average firing rate is stable, providing a conceptual framework for the creation of both the short-term and long-term changes in cerebellar output.

AUTHOR SUMMARY

Activity of the inferior olive, transmitted via climbing fibers to the cerebellum, regulates initiation and amplitude of movements, signals unexpected sensory feedback, and directs cerebellar learning. It is characterized by widespread subthreshold oscillations and synchronization promoted by strong electrotonic coupling. In brain slices, subthreshold oscillations set a temporal framework determining which inputs can be transmitted by inferior olivary neurons and which will not - dependent on the phase of the oscillation. In our study, we tested whether the subthreshold oscillations had any impact on temporal patterning of climbing fiber activity in intact, awake mice. We did so by recording neural activity of the postsynaptic Purkinje cells, in which complex spike firing faithfully represents climbing fiber activity. For short intervals (<300 ms), we found that many Purkinje cells indeed showed spontaneously rhythmic complex spike activity. However, our experiments designed to evoke resonant responses clearly indicated that complex spikes are not predicated on stimulus history. Our realistic network model of the inferior olive explains the experimental findings via continuous phase modulations of the subthreshold oscillations. We conclude that inferior olivary activity is emerging from an aperiodic rhythm, stabilized by electrotonic coupling, and dependent on the behavioral context transmitted via synaptic input.

INTRODUCTION

The inferior olive appears critical for predicting the timing of internally or externally driven inputs (1-3) as well as for generating appropriately timed cerebellar output (4-6). In both cases, timing with the precision of several tens of milliseconds is required across a range of intervals lasting several hundreds of milliseconds (7). Accordingly, clinical manifestations that result from olivary pathology are often associated with impaired timing, as observed in for instance tremor and ataxia (7-12). Although the consequences of dysfunction of the inferior olive are evident, the mechanism by which network dynamics leads to functional behavior is not. The inferior olive is the sole source of the climbing fibers, the activity of which dictates complex spike firing by cerebellar Purkinje cells (for review see De Zeeuw et al. (13)). Climbing fiber activity is essential for motor coordination, as it contributes to both initiation and learning of movements (14-20) and it may be involved in sensory processing and regulating more cognitive tasks (21-23). Understanding the systemic consequences of inferior olivary spiking is therefore of great importance. The dendritic spines of inferior olivary neurons are grouped in glomeruli, in which they are coupled by numerous gap junctions (24-27), which broadcast the activity state of olivary neurons. Due to their specific set of conductances (28-34), the neurons of the inferior olive can produce subthreshold oscillations (STOs) (35-37). The occurrence of STOs does not require gap junctions per se (38), but the gap junctions appear to affect the amplitude of STOs and synchronize them (12, 24, 36). Both experimental and theoretical studies have demonstrated that STOs may mediate phase-dependent gating: the phase of the STO may determine whether excitatory input can or cannot evoke a spike (39, 40). Indeed, whole cell recordings of olivary neurons in the anesthetized preparation indicate that their STOs can contribute to the firing rhythm (36, 37) and extracellular recordings of Purkinje cells in the cerebellar cortex under anesthesia often show periods of complex spike firing around the typical olivary 10 Hz rhythm (41-44). However, several attempts to capture clues to these putative oscillations in the absence of anesthesia have, so far, returned relatively empty handed (45, 46).

It has been shown that in the anesthetized state both the amplitude and phase of the STOs can be altered by synaptic inputs (24). The excitatory inputs to the inferior olive originate predominantly in the spinal cord and lower brainstem, mainly carrying sensory information, and in the nuclei of the meso-diencephalic junction in the higher brainstem, largely carrying higher-order input from the cerebral cortex (Fig. 1A) (7, 47, 48). In addition, the cerebellar nuclei and adjacent nuclei in the hindbrain provide direct inhibitory projections

to the inferior olive (49). Unlike most other brain regions, the inferior olive is virtually devoid of interneurons (50, 51). Thus, the long-range projections to the inferior olive in conjunction with STOs and gap junctions jointly determine the activity pattern of the complex spikes in Purkinje cells. Yet, the relative contributions of intrinsic and extrinsic factors in determining the firing patterns remain to be elucidated.

Fig. 1. *Circuit involved in the production and modulation of complex spikes. (**A**) Simplified scheme of the inputs to the inferior olive (IO). Sensory input reaches the IO directly from the brainstem and spinal cord. In our study, we used facial whisker input that is relayed via the sensory trigeminal nuclei (TN). This input is considered the "sensory input" in our modeling studies. The IO also receives continuous inputs from other brain regions, which we modeled as the "contextual input". The contextual input consists of excitatory input from the cerebral cortex (e.g., the motor (M1) and somatosensory cortex (S1)), either directly or relayed via the nuclei of the meso-diencephalic junction (MDJ), as well as of inhibitory input from the cerebellar nuclei (CN). The output of the IO is exclusively directed to the cerebellum and predominantly to the cerebellar Purkinje cells (PC). Obviously, the sensory input also affects the contextual input indirectly, via the strong pathway from the TN via the thalamus (TH) to the cerebral cortex. (**B**) Representative trace of Purkinje cell activity showing many simple spikes (as downward deflections) and occasional complex spikes (marked with a blue dot). A part of the trace is enlarged in panel (**C**). Recordings were made in awake mice.*

Here, we combine recordings in awake mice – in the presence and absence of gap junctions – and a novel inferior olivary network model to study the functional relevance of STOs in terms of resonant spikes. We are led to propose a view of inferior olivary function that is more consistent with the interplay between STOs, gap junctions and inputs to the inferior olive. Rather than acting as a strictly periodic metronome, the inferior olive appears more adequately described as a ratchet, where cycles with variable periods account for but limited sets of short-lasting periods.

RESULTS

Stimulation promotes oscillatory patterns in profiles of complex spikes over short periods

To study the conditions for, and consequences of, rhythmic activity of the inferior olive, we made single-unit recordings of cerebellar Purkinje cells in lobules crus 1 and crus 2 (n = 52 cells in 36 mice) in the presence and absence of short-duration (30 ms) facial whisker stimulation in awake mice (Fig. 1B-C). Of these cells, we first constructed the inter-complex spike interval (ICSI) histograms during spontaneous activity. In the absence of whisker stimulation, the complex spikes of 35% of the Purkinje cells (18 out of 52) showed rhythmic activity (Fig. 2A-C; S1 Fig.). The median frequency of these spontaneous rhythmic discharges cells was 8.5 Hz (inter-quartile range: 4.7-11.9 Hz). In response to whisker stimulation, 46 out of the 52 cells (88%) showed complex spike responses to whisker stimulation. Of these, 31 (67%) showed sensory-induced rhythmicity (Fig. 2D-F), which was a significantly larger proportion than during spontaneous behavior (p = 0.002; Fisher's exact test). The median frequency of the oscillatory activity following stimulation was 9.1 Hz (inter-quartile range: 7.9-13.3 Hz; (Fig. 2C, F)). Hence, the preferred frequencies in the presence and absence of sensory stimulation were similar (p = 0.22; Wilcoxon rank sum test) (Fig. 2C, F). Typically, complex spike rhythmicity occurred only in a subset of Purkinje cells (spontaneous spiking: 18 out of 52 neurons (35%); stimulus induced: 31 out of 46 (67%) responsive neurons), implying that the regularity of complex spike firing can be easily disrupted. Indeed, of the Purkinje cells that showed complex spike rhythmicity during both spontaneous activity and following stimulation, 9 out of 46 neurons (20%) showed significantly enhanced rhythmic firing following stimulation, according to a Z-score criterion (spontaneous rhythmicity strength: mean Z-score 2.9 ± 1.1. For stimulus induced rhythmicity: 9.7 ± 17.2). The duration of the enhanced rhythmicity following stimulation was relatively short in that it lasted no more than 250 ms. Note that the minimum ICSI interval across cells was 50 ms, putatively representing the refractory period. The average ICSI was 98 ± 40 ms. With our stringent Z-score criterion (>3) a small fraction (2%) of neurons showed 3 rhythmic PSTH peaks. Furthermore, the comparisons between sensory evoked PSTH peaks and spontaneous rhythmicity from CS autocorrelograms in single cells revealed what seemed as consistent frequencies (Fig. 3). From these analyses, we conclude that, although sensory stimulation is not required for the generation of rhythmicity, it does amplify resonant rhythmicity present in spontaneous recordings for short periods of a few hundred milliseconds.

Fig. 2. *Oscillatory dynamics in complex spike firing* in vivo. *(**A**) Representative inter-complex spike-interval (ICSI) histogram of spontaneous firing of a representative Purkinje cell, together with the convolved probability density function and after pruning the peak at 0 ms to improve visibility. The colors of the bins represent the normalized oscillation strength, which were used to create the heat maps of 52 Purkinje cells (**B**). The arrow In **B** indicates the cell taken as illustration in **A**. (**C**) The peak times of the ICSI distributions during spontaneous firing, as observed in **B**, against the Z-scores of these peaks. A Z-score <3 was taken as sign for the absence of rhythmicity (light blue fillings). The pie diagram shows the fraction of Purkinje cells with rhythmic complex spike firing (Z-score > 3; dark blue fillings). (**D**)-(**F**) The same for whisker air puff stimulation-triggered complex spike firing as characterized by a peri-stimulus time histogram (PSTH).*

Fig. 3. *Similarity between spontaneous and sensory-induced rhythmicity. Scatter plot of response peaks intervals versus peak inter-complex spike intervals. Color and size of data points indicate height (in Z-score) of respectively the inter-complex spike interval peak and of the second response peak. Grey scatter-points indicate the data-points falling in the low Z-score (<3) group during spontaneous firing. Note that the colored symbols are preferably located around the identity line.*

Rhythmic patterns of complex spikes following stimulation are semi-periodic but stable

The rhythmicity of the complex spike responses apparent for a couple hundred milliseconds after air puff stimuli was stable across the 1,000 trials (applied at 0.25 Hz) during which we recorded (Fig. 4A-B). For example, the level of rhythmicity of the first 100 trials was not significantly different from that during the last 100 trials (peak amplitude probability was not significantly different, $p = 0.8$; χ^2 test (timing of first peak (mean ± sd): 45 ms ± 5.5 ms and 45 ms ± 6.0 ms, respectively). This strongly indicates that there are – at least in a fraction of the Purkinje cells – persistent temporal windows of opportunity for complex spike firing following a sensory stimulus. To understand to what extent the windows of opportunity for rhythmic firing could be explained by the STOs of the coupled inferior olivary neurons and/or their refractory periods, we ordered trials based on the latency to the first complex spike after the stimulus (Fig. 4C-E). The moments of occurrence of the complex spikes indicated semi-periodic preferred windows of opportunity (as identified with PSTH analysis; windows 30-60 ms; 90-120 ms; 150-190 ms). In this Purkinje cell, 38% of all trials had a response with a complex spike at an average latency of 45 ms during the first window of opportunity (occurring from 30 to 60

ms). In a substantial minority of trials (10%) a complex spike was fired during the second window of opportunity (occurring from 90 to 120 ms), but not during the first window, confirming earlier observations in decerebrate cats (52). Furthermore, in some trials (4%) a complex spike would appear during the third window of opportunity, but not during the first and/or second window (Fig. 4C-E), indicating network wide oscillations. Thus, complex spike firing shows identifiable windows of opportunity of several hundreds of milliseconds for semi-periodic rhythmic firing. These can be evinced by applying sensory stimuli, but these windows cannot be solely explained by a refractory period after an induced complex spike, and hence inferior olivary STOs probably contribute to the semi-periodic timing of climbing fiber activity.

Fig. 4. *Sensory stimulation can induce oscillatory complex spike firing in Purkinje cells of awake mice. (**A**) Whisker air puff stimulation can trigger rhythmic complex spike (CS) firing in Purkinje cells of cerebellar lobules crus 1 and crus 2 of awake mice. This is illustrated by a representative extracellular recording with a stimulation frequency of 0.25 Hz. Two triggered complex spikes are marked according to their order following the stimulus. (**B**) Windows of opportunity for the occurrence of triggered complex spikes become apparent in a raster plot. (**C**) The same data, but now the trials are sorted by the latency of the first complex spike following the stimulus. Note that during trials during which no complex spike is fired during the first window of opportunity, the first complex spike after the stimulus often occurs in the second window of opportunity. (**D**) Peri-stimulus time histogram of complex spikes firing. The bin-width is 10 ms and the blue line shows the convolved histogram with a 5 ms kernel. (**E**) The same peri-stimulus time histogram as in **D**, but now the probabilities of the first, second and third complex spike after the stimulus are shown separately, highlighting the occurrence of windows of opportunity for stimulus-triggered complex spikes.*

Galloping stimuli do not induce conditional spiking

In line with *in vivo* whole cell recordings made under anesthesia (24, 37) our awake data support the possibility that the moment of spiking may be related to the phase of olivary STOs, especially during the period of several hundred ms following stimulation. It is an important question whether the STO is present continuously or only transiently. In order to address this, we designed a 'gallop' stimulation paradigm consisting of stimuli with intervals alternating between durations of 250 ms and 400 ms to distinguish between these two cases. If the impact of the STO rhythm would last longer, the complex spike responses following each stimulus interval

might be expected to show patterns depending on the phase of the STO. Our data do not support the hypothesis that sensory stimuli create phase resets with lasting impact on subsequent spiking. Responses in one interval did not help predict the complex spike firing in the next interval. In none of the 17 Purkinje cells tested in this way the response properties to the 250 ms and 400 ms intervals were significantly different (response ratio for the two stimulus intervals was 0.97 ± 0.23 (average ± sd)). In all Purkinje cells, the response ratios had $p > 0.05$ on Fisher exact test) (Fig. 5A). Neither was conditional dependency observed on a replication with shorter gallop stimulus intervals of 250 ms and 300 ms (S2 Fig.).

Fig. 5. *No phase-dependent spiking probabilities observed* in vivo. *(**A**) In order to test the impact of the presumed phase of the inferior olivary neurons* in vivo, *we applied a "gallop" stimulation pattern, alternating short (250 ms) and long (400 ms) intervals. Air puffs (vertical bars) were delivered to the whisker pad. Complex spikes were counted in response windows (RW) 20-200 ms post-stimulus. Response probabilities were compared between response windows in short and long intervals. The first response window was not included in the analysis because it was not preceded by an air-puff interval. The ratio between number of complex spikes in short and long intervals for the entire population of cells were sorted on the fraction of complex spikes falling in the long response window (indicated as horizontal black lines). For each Purkinje cell the relative response probabilities for the long and short intervals are illustrated as the length of the filled and open bars, respectively. None of the Purkinje cells showed a significant difference in the response probability between the two intervals (all $p > 0.05$ on Fisher's exact test). (**B**) This analysis was repeated, but now including only those response windows that followed a response window with at least one complex spike. This conditional approach (Cond) resulted in similar results as obtained from the analysis of all response windows (All). Shown are the 25 and 75 % quantiles and median per population (see also S3 Fig.). (**C**) If sensory stimulation triggers complex spikes, one would expect that a higher frequency of stimulation would lead to a higher frequency of complex spikes. However, such a relation was absent. For this analysis, we included only sensory-responsive Purkinje cells of which the complex spike response exceeded a bootstrap-derived 99% probability threshold. The gray scaling of the symbols indicates the response probability. Purkinje cells displaying a higher complex spike response rate had a slightly increased firing rate upon higher stimulus frequencies, but this was far from the expected increase (based upon a linear increase; the shaded area indicates the 25-75% probability range).*

Broadly, three cases would encompass the possible causes for olivary spikes causing complex spikes: (1) those that accompany a phase-resetting of the spiking cell, (2) those which are aligned with peaks of the underlying STO rhythm of the single cell, or (3) those that are independent of STO (53). Each of these cases leads to distinct predictions regarding a subsequent spike. We thus thoroughly analyzed the presence of a complex spike as a conditional response of the previous window. For all cells, the probability of response was independent of a spike in the previous window, indicating that the occurrence of the complex spike could not be predicted on the basis of the preceding spike. These analyses led to very similar results (response ratio 0.95 ± 0.4, none of the ratios was found significant ($p < 0.05$) on Fisher's exact test) (Fig. 5B; S3 Fig.). Thus, our *in vivo* data did not exhibit hallmarks of phase-dependent gating in the inferior olive beyond durations of 250 ms -- in stark contrast with the evidence highlighted in Figs. 2, 3 and 4 for the impact of sustained inferior olivary STOs. Thus, the data present a paradox: how can a system with underlying rhythmic responses fail to be phase modulated by periodic stimuli?

Stimulation hardly affects the average firing rate of complex spikes over longer periods

If sensory stimulation can elicit spikes in the inferior olive irrespective of the phase of the STO as suggested by the gallop stimuli (Fig. 5), it is natural to assume that increasing the frequency of stimulation can elevate the average firing frequency of olivary cells. To test this, we subjected Purkinje cells to a wide range of stimulus frequencies, with both regular and gallop patterns. The complex spike frequency was resilient to varying the stimulus frequency between 1 and 4 Hz (linear regression = -0.02; $R^2 = 0.1$; Fig. 5C) and did not show compelling frequency modulation in that neither the spontaneous complex spike firing rate nor the initial response rate had a significant impact on the complex spike frequencies during the various stimulation rates (mean modulation of spiking frequency for all stimulation rates 2% ± 5%). Furthermore, there were virtually no signs of resonance with any of the stimulus frequencies, as there were no frequencies at which the complex spike firing could be substantially increased. Only a very high rate of sensory stimulation (10 Hz), commensurable with the average duration of the short-lasting windows of opportunity described above, could induce an increase in complex spike firing frequency (average increase 71 ± 64% corresponding to an average increase from 1.12 Hz to 1.92 Hz; $n = 5$; $p < 0.05$; *t* test; data not shown). Note that increases in complex spiking frequency signified a reduction in response probability to single stimuli. We conclude that the average

complex spike frequency is robust and stiff to modulation over longer time periods, imposing a hard limit on the frequency with which complex spikes can respond to sensory stimuli.

STOs may contribute to complex spike firing during shorter periods

So far, we found indications for rhythmic complex spike firing for short periods, particularly following sensory stimulation (Fig. 2, 3 and 4), but attempts to reveal phase-dependent responses beyond a few hundred ms after stimulation yielded negative results (Fig. 5). To further assess the relative impact of refractory periods and STOs to the overall firing behavior, we developed a statistical model representing idealized extremes of independent and phase-dependent responses. At one extreme, we examined a linear response model in which sensory stimulus could evoke a complex spike independent of the moment of the last complex spike before that stimulus, apart from a refractory period. This linear response model was contrasted to the other extreme, entailing an oscillatory gating model, where we predicted that the timing of the first complex spike after stimulus onset would be in-phase with an ongoing oscillation. The frequencies of the oscillations were deduced for each Purkinje cell individually by a combination of the peaks in auto-correlograms and the stimulus-induced oscillations, described above. For each Purkinje cell we compared the distribution of the intervals between the last complex spike before and the first complex spike after stimulus onset with the predicted distributions based on the linear model, the oscillatory model and nine intermediate models, mixing linear and oscillatory components with different relative weights (Fig. 6A-E). For the two extreme models as well as for the nine intermediate models we calculated a goodness-of-fit per Purkinje cell. Overall, when using these relatively long periods (300 ms) the linear model was far superior to the oscillatory model, although a minor oscillatory contribution could often improve the goodness-of-fit (Fig. 6F-H). Hence, the failure and success of the models to predict rhythmicity over longer and shorter periods, respectively, further confirms the observation that a stable STO frequency is unlikely, despite what is indicated by prominent autocorrelation side-peaks.

Fig. 6. *Sensory stimulation leads to unconditional complex spike responses* in vivo. *(**A**) We quantified the impact of ongoing subthreshold oscillations on the occurrence and timing of complex spikes by comparing the cross-stimulus interval between the last complex spike before and the first complex spike after a sensory stimulus to the preferred firing frequency of each individual Purkinje cell. This approach is illustrated by the analysis of a single,*

*representative Purkinje cell: the data in **A**-**E** originate from the same cell. A representative trace is shown in (**A**) and enlarged in (**B**), showing the cross-stimulus interval as a horizontal red line. (**C**) For each Purkinje cell, we first established the preferred firing rates based upon the auto-correlogram (**C**) and the peri-stimulus time histogram (**D**; cf. Fig. 2). The histograms were convolved with an Epanechnikov kernel. The intervals between the last complex spike before and the first complex spike after the stimulus for each trial yielded for each neuron a curve (red line). The observed probability density function was compared with calculated probability density functions based upon predicted firing as derived from a uniform complex spike distribution (dotted line), an oscillatory complex spike distribution (blue line) and 9 intermediate models that were combinations of these two extremes with different relative weights. (**F**) The distributions of the goodness-of-fit for each of the 11 models showed a clear bias towards the uniform model, refuting the impact of subthreshold oscillations on sensory-induced complex spike firing. Each model was run 1,000 times. The middle line indicates the average of all runs, the upper and lower lines indicate 75 and 25% quantiles. (**G**) Distributions of the goodness-of-fit of all Purkinje cells that showed clear rhythmicity, but nevertheless had better matches with the uniform firing model. (**H**) Histograms of the maxima in the distributions shown in **G** confirm that the impact of the subthreshold oscillations on sensory CS responses is minimal.*

Gap junctions facilitate frequency modulation of rhythmic complex spike firing

Apart from the STOs, extensive gap junctional coupling between dendrites is a second defining feature of the cyto-architecture of the inferior olive (27, 54). Absence of these gap junctions leads to relatively mild, but present behavioral deficits in reflex-like behavior and learning thereof (24, 55). We analyzed during spontaneous activity the inter-complex spike interval times in Purkinje cells of mutant mice that lack the Gjd2 protein and are hence unable to form functional gap junctions in their inferior olive (56). Perhaps surprisingly, the absence of gap junctions did not quench rhythmic complex spike firing, which was still prominent in the absence of gap junctions (Fig. 7A). In fact, the fraction of Purkinje cells showing significant rhythmicity in the Gjd2 KO mice was larger than that in the wild-type littermates (Gjd2 KO: 38 out of 65 Purkinje cells (58%) vs. WT: 15 out of 46 Purkinje cells (33%); p = 0.0118; Fisher's exact test), with their average rhythmicity being significantly stronger (p = 0.003; Kolmogorov-Smirnov test), measured by Z-scores of side peaks (Fig. 7B). Indeed, the variation in oscillatory frequencies across Purkinje cells of the mutants was significantly less than that in their wild-type littermates in that the latency to peak times per Purkinje cell were less variable (p =

0.0431; Mann-Whitney test; Fig. 7C). Thus, gap junctions in the inferior olive are not necessary for the occurrence of rhythms, while they do lead to a wider distribution of the frequency of the rhythmic firing.

Fig. 7. *Oscillatory dynamics in spontaneous firing in vivo in the presence and absence of gap junctions. (**A**) Color-coded inter-complex spike-interval (ICSI) histogram of spontaneous firing of 60 Gjd2$^{-/-}$ and 52 wild-type Purkinje cells. (**B**) The Gdj2$^{-/-}$ Purkinje cell distribution shows higher Z-scores than the wild-type population, indicating a stronger rhythmicity during spontaneous firing in the absence of gap junctions (p = 0.003; Kolmogorov-Smirnov test). A Z-score >3 was taken as sign for the presence of rhythmicity – which occurred more often in the Gjd2 KO than in the WT Purkinje cells (colored fraction in the pie diagrams; p = 0.005; Fisher's exact test). In the absence of gap junctions, rhythmic firing was more stereotypical, as illustrated by less variation in the time to peak (**C;** p = 0.0431; U = 1030.0; Mann-Whitney test). Note that the left panel of **A** is a copy of Fig. 2B and presented here to facilitate comparison.*

Temporal relations of complex spikes of different Purkinje cells

We made paired recordings of Purkinje cells in crus 1 and crus 2 to study the temporal relations of their complex spikes during spontaneous activity. The cell pairs were recorded with two electrodes randomly placed in a grid of 8 x 4, with 300 micrometers between electrode centers. Cell pairs showed coherent activity in that they could show a central peak and/or a side peak in their cross-correlogram (Fig. 8A-C). The side peaks could appear at different latencies, similar to the range observed in autocorrelograms of single Purkinje cells (cf. Fig. 2B). Moreover, Purkinje cell pairs that did not produce signs of synchronous spiking in the center peak could still produce an "echo" in the side peak after 50-150 ms. Counter-intuitively, cross-correlograms of Purkinje cell pairs of the wild type mice showed less often a significant center peak than those of Gjd2 KOs (WT: 51 out of 96 pairs (53%; N = 4 mice); Gjd2 KO: 44 out of 61 pairs (72%; N = 7 mice); p = 0.0305; Fisher's exact test), while the strength of the center peak was on average enhanced in the absence of gap junctional coupling (Z scores of significant center peaks (median ± inter-quartile range): WT: 3.47 ± 1.82; Gjd2 KO: 5.75 ± 5.58; p = 0.0002; Mann-Whitney test)) (Fig. 8D-F). Instead, the side peak of Gjd2 KO Purkinje cell pairs was not stronger than that of WTs (Z scores of significant side peaks (median ± inter-quartile range): WT: 3.01 ± 0.89; Gjd2 KO: 3.04 ± 1.52; p = 0.194; Mann-Whitney test), leading to a lower ratio between center and side peak (mean ± SEM: WT: 90.70 ± 5.17%; Gjd2 KO: 72.86 ± 6.52%; p = 0.036; t = 2.143; df = 67; t test).) (Fig. 8E-F). Interestingly, the

occurrence of side peaks in Purkinje cell pairs was unidirectional in approximately half the cell pairs (WT: 47 out of 82 pairs with at least one side peak (57%); Gjd2 KO: 25 out of 47 pairs (53%); $p = 0.714$; Fisher's exact test), which means that one of the neurons of a pair was leading the other, but not vice versa. As this was consistent in the Gjd2 KO and in the WT Purkinje cells, these data could reflect traveling waves across the inferior olive, which, however, must have extrinsic sources (38, 57). Thus, the paired recordings are compatible with the findings highlighted above that the presence of coupling can affect the coherence of STOs for short periods up to a few hundred milliseconds, while leaving the window for later correlated events open.

Fig. 8. *Coherence of complex spike firing of Purkinje cells over time. Two Purkinje cells recorded simultaneously in a wild-type (WT) mouse during spontaneous activity, showing an epoch with near-synchronous complex spike firing with both spikes in the center-time interval (**A**), or another epoch at which the same cells fired temporally further apart with one complex spike in the center-time and another one in the side-peak interval (**B**), leading to a double-peaked cross-correlogram for this cell pair (**C**). (**D**) Heat map representations of cross-correlograms between simultaneously recorded Purkinje cells in WTs and Gjd2 KOs. Note the stronger impact of the center peak in Gjd2 KO mice compared to WT mice. However, the side peak, the latency of which was used to order the cell pairs, is stronger in WT pairs. The side peak can be regarded as a "network echo". (**E**) Venn diagrams showing the relative occurrence of center and side peaks in the presence and absence of gap junctions. (**F**) In the absence of gap junctions, the center peak, but not the side peak, was stronger (left and middle panel). Likewise, the normalized ratio of the side peak vs that of the center peak was lower in the Gjd2 KO mice (right panel). * and *** indicate $p < 0.05$ and $p < 0.001$, respectively (t test).*

Inferior olivary network model suggests semi-periodic STO behavior

Our experimental data provided evidence for the existence of inferior olivary STOs in the awake brain, but galloping stimuli failed to produce conditional spiking as expected from phase dependencies. Thus, while STOs could explain the rhythmicity of complex spike firing remaining stable for the duration of our recordings, it concerned short periods of all but a few hundred ms given sensory input. Gap junctions, instead of creating more uniform complex spike patterns, proved to create more diverse patterns, which appear to also have an impact on the global network activity. To study the mechanisms underlying these findings, we developed a tissue-scale network model of the inferior olivary neuropil, composed of 200 biophysically plausible model

cells (34, 40, 58) (Fig. 9A) embedded in a topographically arranged 3D-grid (Figure 9B). The model is aimed at testing hypotheses on the putative impact of STOs, physiological parameters, gap junctions and synaptic inputs on the generation of patterns of complex spikes.

Fig. 9. *A realistic network model of the inferior olive. (**A**) To study the relative impact of the different components of the inferior olive we employed a biologically realistic network consisting of 200 model neurons. The model neurons received input from two sources: a coupled, phasic input mimicking sensory input. The "sensory input" reaches a subset of neurons synchronously and with equal strength. The "sensory input" is complemented with a continuous input that is a mixture of excitatory and inhibitory synapses representing feedback signals from different sources, providing a functional context to the inferior olive. This "contextual input" is modeled as an Ornstein-Uhlenbeck (OU) noise process delivered to all neurons in the model network with a 20% correlation over time. As in the biological counterpart, the model neurons are interconnected by gap junctions. (**B**) The model neurons display subthreshold membrane oscillations (STOs), represented by the lower circle, and spiking, represented by the upper circle. The colors indicate which current dominates which part of the activity pattern: I_h current (green), a hyperpolarization-activated cation current, underlies a rise in membrane potential. Subsequently the I_t current (red), mediated by low threshold T-type Ca^{2+} channels, further drives up the membrane potential and from here either the sub-threshold oscillation continues (lower circle) or a spike is generated (upper circle), mediated though I_{Na} and I_K currents (yellow and blue, respectively). Both after a spike or a subthreshold peak, influx of Ca^{2+} will trigger the activation of the hyperpolarizing K^+ current by Ca^{2+}-dependent K^+ channels (blue). This hyperpolarization will again activate the I_h current starting the oscillation cycle again. A resulting trace of the subthreshold membrane potential oscillation punctuated with one spike is shown on the right. (**C**) 3D connectivity scheme of the 200 neurons in the network model. Links indicate gap junctional interconnections; the color of each neuron in the model represents the number of neurons to which that cell is connected through gap junctions. The thick green lines indicate first and second order neighbors of the center cell as an example. (**D-E**) Membrane potential of cells in the absence of input, for networks with and without coupling. (**F-G**) Cell activity sorted by amplitude, indicating that coupling the networks bring many cells into oscillating. (**H-I**) Distribution of STO frequency and amplitude for coupled (with gap junctions) and uncoupled (without gap junctions) model networks.*

Our network model includes 200 neurons in a 3D-grid arrangement (Fig. 9B), representing a sheet of neurons of about 10% of the murine principal olivary nucleus (59). Each neuron in the model is composed of somatic, axonal and dendritic compartments, endowed with a particular set of conductances, including a somatic low threshold Ca^{2+}channel ($Ca_v3.1$), and a dendritic Ca^{2+}-activated K^+ channel, chiefly regulating STO amplitudes, while a somatic HCN channel partially determines the STO period (Fig. 9; see also Methods). The dendrites of each neuron are connected to the dendrites of, on average, eight nearby neighbors (within a radius of 3 nodes in the grid, representing a range of about 150 µm of the murine inferior olive), simulating anisotropic and local gap junctional coupling. The coupling coefficient between model cells varied between 0 and 10%, as reported from experimental data (39, 60, 61). Sensory input was implemented as "excitatory synaptic input (AMPA)", reflecting the whisker signals originating from the trigeminal nuclei that were synchronously delivered to a subset of model neurons. Additionally, a "contextual input" was implemented as a combination of inhibitory feedback from the cerebellar nuclei and a level setting modulating input like that from the nuclei of the meso-diencephalic junction (Fig. 1A and 9A). This contextual input is modeled after an Ohrstein-Uhlenbeck process; essentially a random walk with a decay parameter which imposes a well-defined mean and parameterizable temporal correlations (see Methods). The amplitude of the contextual input drives the firing rate of the model neurons, which we set around 1 Hz (Fig. S4, S5), corresponding to what has been observed *in vivo* (62). An extensive parameter space exploration of the contextual input ensured that the model network operated within realistic boundaries in that the incoming and resulting frequencies predicted by the model are supported by the current and previous experimental data (Fig. S4, S5) (22, 37). Thus, our model network recapitulates at least part of the neural behavior observed *in vivo* due to biophysically plausible settings of intrinsic conductances, gap junctional coupling and synaptic inputs.

Characteristics of STO dependent spiking in the network model

Whether a model neuron at rest displays STOs or not is largely determined by its channel conductances. Activation of somatic T-type Ca^{2+} channels can trigger dendritic Ca^{2+}-dependent K^+ channels that can induce I_h, which in turn can again activate T-type Ca^{2+} channels, and so forth. This cyclic pattern can cause STOs that could occasionally produce spikes (Fig. 9C). The conductance parameters were randomized (within limits, see Methods) to obtain an approximate 1:3 ratio of oscillating to non-oscillating cells (S5 Fig.) guided by

proportions observed *in vivo* (37). Sensitivity analysis with smaller ratios (down to 1:5) did not qualitatively alter the results (data available online, see https://osf.io/6x5uy/).

In the absence of "contextual input", model neurons were relatively silent, but when triggered by "sensory input", as occurred in our behavioral data (Fig. 2 and 4), STOs synchronized by gap junctions would occur for two or three cycles (Fig. 10A). Our network model confirms that gap junctional coupling can broaden the distribution of STO frequencies and that even non-oscillating cells may, when coupled, collectively act as oscillators (S6 Fig.) (63). Adding "contextual input" to the model network can lead to more "spontaneous" spiking in between two sensory stimuli. Compared to the situation in the absence of "contextual input", the STOs are much less prominent and the post-spike reverberation is even shorter (Fig. 10B). Accordingly, despite the significant levels of input correlation (10%) in the "contextual input", the periods between oscillations are more variable due to the interaction of the noisy current and the phase response properties of the network. In addition, in the presence of "contextual input" our model could readily reproduce the appearance of preferred time windows for spiking upon sensory stimulation as observed *in vivo* (cf. Fig. 4). This was particularly true for the model cells that directly received "sensory inputs" (Fig. 10C-D). Moreover, the observed rhythmicity in model cells as observed in their STO activity was in tune with that of the autocorrelogram (Fig. 10E) in that the timing of the STOs and that of the spiking were closely correlated (cf. Fig. 9C). It should be noted though that model cells adjacent to cells directly receiving "sensory input" showed only a minor effect of stimulation. Thus, even though the gap junction currents in the model were chosen to as the ceiling physiological value for the coupling coefficient (≤10%) (39, 63), these currents alone were not enough to trigger spikes in neighboring cells.

Fig. 10. *Synaptic input strongly affects the oscillatory behavior in a network model of the inferior olive. (**A**) A phasic and synchronous input mimicking sensory input (see Fig. 9A) was delivered to a subset of cells (indicated in red) of the model network. Membrane potentials of all 200 cells in the model network in the absence of "contextual input" (see Fig. 9A). Pink traces represent the membrane potentials of cells directly stimulated by the "sensory input" (see **A**), with the red trace being their average. Below are the membrane potentials of the model cells as a heat map. Each row represents one model cell and the small circles indicate the occurrence of spikes. In the absence of "contextual input", model neurons displayed long lived and regular transient subthreshold oscillations following each "sensory input". These patterns changed dramatically, however, after adding*

*"contextual input". This "contextual input" models the combination of inhibitory and excitatory inputs from other brain regions to the inferior olive (**B**). While in the absence of "contextual input", model neurons showed synchronous subthreshold oscillations and were silent except upon receiving "sensory input", now – in the presence of "contextual input" – spikes occur throughout the simulation and the subthreshold oscillations are unstable and not synchronized. Note that despite the largely uncorrelated "contextual input", model cells did not fire homogenously, but loose clusters were present. (**C**) Rhythmic responses to stimulation are reproduced by the inferior olivary network model. From the model network, we present a cell with responses to "sensory input" that reproduce oscillatory features of the PSTH and autocorrelogram as found in vivo (see Fig. 4). Raster plot of olivary spiking triggered by 182 stimuli ("sensory input"), ordered by latency to the first spike following the stimulus. As seen in the in vivo data, the first spike after the stimulus can fall in multiple windows of opportunity. For this simulation, we included the "contextual input". (**D**) Peri-stimulus time histogram showing the response peaks upon "sensory input". (**E**) Autocorrelograms comparing spikes produced during stimulation with spikes due to background (spontaneous) activity. Periodic stimulus delivered to the network reduced resonant response at the peak. The extreme short-latency responses (in the center of the autocorrelogram) are due to spikelets that can also be seen in **C**. (**F**) Raster plot like in **C**, but with overlaying membrane potentials. For clarity, only the first 50 stimuli are displayed. Spike symbols follow conventions in **C**. Trials with low latency were preceded by a dip in the preceding membrane potential, a phenomenon that can also be clearly observed in **G** and **H**. (**G**) Average membrane potential of this neuron aligned by spikes that were either due to "sensory input" (19 spikes; red) or produced spontaneously (61 spikes; blue). The light shaded backgrounds represent the 10% and 90% percentile ranges of membrane potential. Dips in membrane potentials preceding spike reveal that for both groups a prior inhibition increased the probability of spiking. Importantly except for a refractory period, we did not observe a clear oscillation pattern following either spike type, due to variability imposed by the "contextual input". (**H**) Average membrane potential traces of this neuron aligned to stimulus, separating trials with from trials without a spike. Clearly, stimulus-evoked spikes were most likely related to preceding dips in the membrane potential.*

Both directly stimulated model cells and those receiving only "contextual input" displayed a preference for phase, which can be seen in the spike-triggered membrane potential average as well as in the spike-triggered average of the input currents (Fig. 10F-H). Spike-triggered averages of membrane potential for any cell clearly showed hyperpolarization, indicating a preference for a preceding phase. In contrast, trials in which no spike

was generated showed a depolarization just before the occurrence of the input. Similarly, the average of the input showed a long-lived phase preference, not only for a hyperpolarization before the spike, but also a preference for a depolarization in the previous peak of the STO, more than 100 ms earlier. Thus, in line with the experimental data, the model indicates that for short durations STOs can induce clear phase dependencies for spiking, but over multiple trials this effect fades in the variation of period durations dependent on the trial-specific "contextual input".

Phase-dependent gating in the network model

Depolarizing "sensory input" delivered onto a subset of the model cells can reset the STO phase in oscillatory cells and create resonant transients in others (Fig. 11A-B). If a second stimulus was delivered during this short-lasting transient, the response was clearly phase-dependent. As in most cells with resonant short-lasting dynamics, inputs delivered during different phases can cause phase shifts in different directions. Hyperpolarization advanced the phase between 0-π and delayed the phase between π-2π, while depolarization had roughly the opposite effect, in addition to phase advancements with spikes in later phases between π-2π (Fig. 11C-F). Thus, there is a mutual influence of synaptic input and STOs on periodicity. While STOs can lead to phase-dependent gating, synaptic input can either modulate or reset the phase of the STOs, generating variable periods that range between 40-160 ms for the chosen "contextual input" amplitude (Fig. 12; S6 Fig.).

Fig. 11 *Synaptic input determines the phase-dependent gating properties of the inferior olive network model. (**A**) Phase-dependent spiking was very prominent in our network model of the inferior olive in the absence of "contextual input". We repeatedly stimulated the same 54 model cells with synchronous "sensory input" (cf. Fig. 9A). The other 146 neurons of the network model were present, but not stimulated. The phase-dependent gating was studied using tandem stimulation with varying inter-stimulus intervals. The membrane potential of each of these 54 model neurons is plotted in **A** as a waterfall plot and in **B** as a heat map. The simulations are grouped by the interval between the two stimuli, starting with a single stimulation (bottom, red), and continuing with small to large intervals. In 13 equal steps two whole cycles of the subthreshold oscillation were covered. (**C**) Average and inter-quartile range (shaded area) of membrane potentials of neurons in the network that were only perturbed once at 0 ms ("red perturbation group" in **A** and **B**). The phase of the subthreshold oscillations of the*

*"synchronized" cells in the network was used to compute the data displayed in **D** and **E.** (**D**) Spike probability plot as measured for the second perturbation at the different phases of the membrane oscillation. Spike probability was computed as the number of neurons firing divided over the total number of neurons getting input. The first perturbation given at the peak of the oscillation is demarked as the start of the oscillation cycle. We see that secondary perturbations at both a half and one-and-a half cycle (pi and 3pi, respectively) did not trigger spikes, while perturbations following at either one or two full oscillation cycles (2π and 4π, respectively) did trigger spikes. The repetition of the 'sinusoidal' probability curve shows that the spiking impediment is not (only) due to a refractory period, but follows the phase of the oscillation, being in more hyperpolarized states (not shown). (**E**) Phase response curve showing that perturbations early in the oscillation phase did not impact much on the timing of the spike, but halfway the oscillation the perturbations advanced the ongoing phase considerably which declined linearly to the end of the full cycle. The average membrane potential at the perturbation at 0 ms only went up to -15 mV and not up to the average spike height of approximately 10 mV, because in the population making up the average not all neurons spiked. (**G**) In order to test the impact of the presumed phase of the inferior olivary neurons, we applied a "gallop" stimulation pattern, alternating short (250 ms) and long (400 ms) intervals. "Sensory input" (vertical grey bars) were delivered and complex spikes were counted in response windows (RW) 0-180 ms post-stimulus. Response probabilities were compared between RWs in short and long intervals. The first response window is not included in the analysis because it is not preceded by a stimulus interval.*

Fig. 12. *Significant variability of oscillatory periods induced by contextual input on oscillation period of a single model cell. (**A**) Distribution of inter-peak intervals for a single model cell under 5 s of contextual stimulus of different amplitudes. To gauge period variability without introducing refractory periods, input levels were chosen for non-spiking subthreshold dynamics only. The unperturbed model cell (in black) produces regular periods, while weak contextual stimulus is sufficient to create substantial variability (red and blue). (**B**) Example traces of membrane potential and (**C**) phase for the single cell under perturbations, for the same random seed. Note that under contextual input there was substantial variation in periods, but similar STO periodicity despite different levels of input.*

To find out whether the STOs might also have longer-term impact beyond a few hundred ms, we reproduced in the model the conditions of the "gallop stimulus" experiment, consisting of alternating 250 ms and 400 ms

stimulus intervals (Fig. 11F). We compared the resulting probabilities of observing spikes in the short or long interval in the presence and absence of contextual input. In the absence of "contextual input", a large number of model cells (16 out of 45 spiking neurons, i.e. 36%) receiving direct "sensory input" produced spikes exclusively following either one of the two intervals. In the presence of contextual input, only 5 out of the 200 spiking neurons had preferred windows. This outcome closely resembles the experimental data on the distribution of firing probabilities for spikes following the same gallop stimulation (compare Fig. 5A with Fig. 11F), highlighting the fact that conditional dependence of spiking is largely quenched in the presence of synaptic noise from an active brain.

Model shows activity networks that are stable and oscillating, but semi-periodic

In line with the experimental *in vivo* data (e.g., Fig. 2 and 4), the olivary spike rhythmicity in the network model was steadily present over longer periods, and for a wide range of "contextual input" parameters of spatial and temporal correlation (S4 Fig.). In addition, it also comprised, as in the experimental data, variations in frequency and amplitude during shorter epochs (Fig. 13 and S6). Analysis of the network parameters indicates that these latter variations in oscillatory behavior can be readily understood by their sensitivity to both the amplitude (parameter 'sigma') and kinetics (parameter 'tau', temporal decay) of the "contextual input". Indeed, because of the underlying Ornstein-Uhlenbeck process, the generation of "contextual input" converges to a specified mean and standard deviation, but in short intervals the statistics including the average network STO frequency can drift considerably (Fig. 10B and Fig. 12). Since relatively small differences in oscillation parameters such as frequency and periods can accumulate, they can swiftly overrule longer-term dependencies created by periodically resetting stimuli, as an analysis of phase distributions to stimulus shows (Fig. 13). Thus, based upon the similar outcomes of the network model and *in vivo* experiments, we are led to propose that (1) the STOs in the inferior olive may well contribute to the continuous generation of short-lasting patterns of complex spikes in awake behaving animals, and that (2) the synaptic input to the inferior olive may modify the main parameters of these STOs. Note that in the absence of input, periodic rhythmic behavior should be the default behavior of oscillating cells. Thus, in all likelihood, even if the inferior olive oscillates endemically, sustained but variable input should induce highly contextual spike responses to variable periods (hence rendering the olivary responses semi-periodic), rather than stiff periodic rhythms.

Fig. 13. *Impact of periodic stimulation on network phase in the presence of contextual stimuli for networks with (left column) and without gap junctions (right column). Gray bars indicate stimulation time.* ***(A)*** *Stimulus triggered membrane potential for all cells in the network (N=100 stimuli). Stimulation causes a peak in the membrane potential of the directly stimulated cells (mask). The effect of the current spreading through gap junctions is visible in the cells immediately neighboring the stimulated cells (green line), while it was absent in the network model without gap junctions.* ***(B)*** *Increase of synchrony in the network due to a single stimulus. Synchrony is displayed as phase concentration over time (the Kuramoto parameter) for cells under the stimulation mask (colored) and other cells (gray). Stimulation generated a transient synchrony peak in both networks but is considerably higher and longer lived in cells with gap junctions, due to synchrony inducing current flows.* ***(C)*** *Polar plots indicating network phase distribution for snapshots (arrows) for stimulated (colored distribution) and non-stimulated cells (gray distribution). Phase alignment of subthreshold oscillations of the inferior olivary network model was reduced in the absence of gap junctions.* ***(D)*** *Phase distribution of cells over time. Color code represents the proportion of neurons occupying a certain phase at a given time (phase bin size is 2pi/100, time bin is 1 ms). Dark/Light bands indicate that the phase alignment propagates to most cells in the network and subsists for longer durations for the WT network. Nevertheless, "contextual input" overruled the phase alignment within a few hundred milliseconds (~300 ms in this case). In the absence of gap junctions, the impact of the stimulus is restricted to stimulated cells, so that the coherence induced by stimulus on the network was much smaller.* ***(E)*** *Same as D but displaying averaged phase distributions from 100 stimuli. After 200 ms the effect of the stimulus was hardly noticeable, and there was no indication of entrainment, which would be visible as vertical bands before the stimulus. This is because the effect of the stimulus is not stereotypical, due to dependency on network state and contextual input (see also Fig. 11).* ***(F)*** *Average network synchrony triggered on the stimulus. The horizontal lines in the bottom plot are the 95% inclusion boundaries taken from the 5 s of spontaneous network behavior to contextual input (no periodic "sensory" pulses). The model network with gap junctions displayed an elevated synchrony plateau after the stimulus, which ended after around about 200ms, disappearing visibly earlier in the absence of gap junctions. There was no preceding synchrony, indicating complete absence of entrainment to the periodic stimulus.*

DISCUSSION

Given the major impact of complex spikes on Purkinje cell processing and motor behavior (8, 18, 24, 64, 65), resolving the mechanisms underlying their timing is critical to understand the role of the olivocerebellar system in motor coordination. Synchronized subthreshold oscillations (STOs) of olivary neurons have been suggested to contribute to the formation of temporal patterning of complex spike firing, but most of the evidence for STOs has been obtained in decerebrate or anesthetized animals *in vivo* or, even more indirectly, *in vitro* (24, 35-37, 39, 42, 66), but see Ebner and Bloedel (67). To address the question as to whether the effects of STOs can induce resonant effects of Purkinje cell complex spike firing in the awake brain, we evaluated rhythmic complex spike firing in intact behaving animals responding to peripheral stimuli and we investigated to what extent these experimental data are in line with simulations run on a tissue-scale model of the inferior olivary network. Our experimental results indicate that inferior olivary STOs persist in the intact awake brain and are reflected in the temporal patterning of complex spikes for short periods of a few hundred milliseconds following stimulation. However, given the lack of resonant responses over longer time windows and given the inconsistency of individual olivary cells to fire on every trial or cycle, the STOs do not appear regularly periodic, but rather semi-periodic, while still being synchronous, at least at the scale of a few hundred neighboring cells. The model indicates that the periodicity of the STOs of an olivary neuron and network can be readily disrupted or modified when it receives active synaptic inputs from other brain regions, an effect that is consistent with its known phase response properties (40, 63). Thus, our integrated experimental and modeling approach allowed us to shed light on how inferior olivary STOs may contribute to the patterning of synchronous complex spike firing of cerebellar Purkinje cells in a context-dependent fashion.

Complex spike patterns are explained by cell physiology and network-wide properties

Complex spikes have been bestowed with a plethora of functions, including induction of synaptic plasticity, motor learning, as well as motion initiation (13, 68). During spontaneous activity Purkinje cells generally fire a complex spike only once a second, but this frequency can be increased to about 10 Hz by systemically applying drugs, like harmaline, which directly affect conductances mediating STOs in the olive (35, 69). Since these drugs also induce tremorgenic movements beating at similar frequencies, it has been proposed that the inferior olive may serve as a temporal framework for motor coordination (8, 70). This oscillatory firing behavior of the olivary neurons may mirror limb resonant properties and act as an inverse controller, for example by dampening the dynamics of the muscles involved as in the proposal by Alvarez-Icaza and Boahen (71).

As shown before (15-17, 22, 64, 68, 72-74), the current data also show that it is a tiny minority of Purkinje neurons that produce sensory-induced complex spike responses with probabilities larger than 50%, and this probability falls substantially with increasing frequency of stimulation, although the overall spike frequency marginally increases to high frequency stimulation. Moreover, even after applying different temporal patterns of sensory stimulation for longer epochs, we failed to induce a substantial deviation from the stereotypic 1 Hz firing rate. Evinced by this behavior is a strong homeostatic mechanism keeping the complex spike rate relatively stable over longer time periods (74), irrespective of an enduring powerful sensory stimulus. The presence of a complex spike in an interval is compensated by the absence in another, thus it looks as if the complex spikes rearrange themselves in time in order to keep close to the 1 Hz frequency. It remains to be shown to what extent the source of this powerful homeostatic mechanism is intrinsic (cell-dependent) or extrinsic (network-dependent). An interesting intrinsic candidate for setting the overall level of excitability is given by the Ca^{2+}-activated Cl^{-} channels, which are prominently expressed in the inferior olive along with Ca^{2+}-dependent BK and SK K^{+} channels (75). With regard to the extrinsic mechanisms, it should be noted that the overall modulatory effect to stimulation frequency is very resilient, despite the fact that the limiting effect of the complex spike refractory period on its rate would allow higher discharge rates (surely up to 10 Hz). So, why does the olivary firing rate not remain high at larger stimulation frequencies for longer durations, despite the resonances observed in the olivary system? One candidate mechanism could be the homeostatic role conveyed within the olivocerebellar module itself (76, 77). Indeed, the long-term dynamics within the closed olivo-Purkinje-cerebellar nuclei loop may well exert homeostatic control, given that increases in complex spikes lead to enhanced inhibition of the olive via the cerebellar nuclei. The impact of

such a network mechanism may even be more prominent when changes in synchrony are taken into account. We contend that a closed-loop experiment, which would generate sensory stimulation as a function of the degree of complex spike synchrony, could show related conditional probabilities of complex spikes, and perhaps further elucidate how homeostatic control of inferior olivary firing may come about.

Inferior olivary STOs

Our findings on the existence of temporal windows for complex spike responses following stimulation highlighted the potential impact of STOs on conditional complex spike gating (24, 35, 37, 78). Moreover, comparing actual firing patterns and statistical models based on linear or oscillatory interval distributions also indicated a potential impact of oscillations. Our modeling data suggest that asynchronous inputs, such as those mediating inhibition from the cerebellar nuclei in the hindbrain or those relaying depolarizing modulation from the raphe nuclei (79, 80), may induce minor variations in the oscillation time on a cycle-by-cycle basis, even when induced at the subthreshold level (Figs. 11 and 12). As these contextual inputs are absent or suppressed in decerebrate or anesthetized preparations as well as *in vitro*, they may also explain why many earlier studies systematically encountered more stable STO frequencies (24, 35, 37, 39, 42, 53, 66, 81). In our model, in which we mimicked the contextual input as an Ornstein-Uhlenbeck process, with local variations but no long-term drifts of the mean (82), the results agree well with the experimental observations in terms of synchronous firing, phase shifts and overall firing frequency.

The role of gap junctions in complex spike timing

Apart from the almost complete absence of interneurons, the presence of STOs and the exclusive projection to the cerebellum, the abundance of dendro-dendritic gap junctions is another defining feature of the inferior olive. The absence of these gap junctions does not lead to gross motor deficits but prevents proper acquisition and execution of more challenging tasks (12, 24, 55), which is in line with the relatively minor impact found on complex spike activity in Gjd2 KO mice (Fig. 10B). At first sight, the effect of deleting gap junctions seems counterintuitive. Synchronous and rhythmic patterns are exaggerated, rather than diminished by the loss of gap junctions (Fig. 7). Gap junctions do not only facilitate synchronization of coupled neurons, they also lower their excitability by increasing the membrane capacitance (56). Together, this results in less direct coupling, observed as reduced synchrony of direct neighbors (12, 83), and increased responsiveness to synaptic input.

This leads to more long-range synchrony (Fig. 8). Thus, the gap junctions may act as a "noise filter", making the inferior olive more robust and promoting short-range quorum-voting on phase, a term coined by Winfree (84), to summarize the effect of local coupling. This is in line with the finding that complex spikes of nearby Purkinje cells have strong preference to fire together even in the absence of sensory input (85, 86). Moreover, this concept also agrees with the possibility that coupled olivary neurons may control movements by dampening the dynamics of the muscles involved at an appropriate level (71, 87), as both the OSTs and movement oscillations increase shortly after sensory stimulation in Gjd2 KO mice (12).

Reverberating loops

In addition to the autochthonous dynamics of the inferior olive, reverberating loops through the circuit could help explain some features of complex spike firing, including the occurrence of complex spike doublets and side lobes in cross-correlograms. Such phenomena could be explained by "network echos", where complex spikes in one cycle would induce complex spikes in the next cycle. The most obvious candidate loop to produce is that via the cerebellum and the nuclei of the meso-diencephalic junction (48, 88). The output of the inferior olive is exclusively directed to the cerebellum and in particular via exceptionally strong synapses to the Purkinje cells (89). These Purkinje cells in turn inhibit neurons of the cerebellar nuclei that can show rebound firing after a period of inhibition (77, 90). This rebound activity can excite the inferior olive again via a disynaptic connection via the nuclei of the meso-diencephalic junction. While an isolated complex spike is unlikely to evoke such a rebound activity, a larger group of Purkinje cells could be successful in doing so (13, 90, 91). The travel time for this loop (around 50-100 ms) has been indirectly assessed in the awake preparation (19, 20, 24), and corresponds to the latency of the rebound firing in the cerebellar nuclei under anesthesia (76, 77, 90, 92). This implies that the travel times for the entire loop would be in the same order as found for the preferred frequencies of complex spike firing. Other, more elaborate loops involving for instance the forebrain also exist (93) and could play an additional role in shaping complex spike patterns.

A putative impact of reverberating loops on rebound activity could be a network phenomenon, as the impact of an isolated complex spike would not be sufficient to trigger this loop. This is in line with the reduced "echo" in the cross-correlograms of the Gjd2 KO mice (Fig. 8) and enhanced doublets following lesions of the nucleo-olivary tract as occurs in olivary hypertrophy (94). Taken together, refractory periods, STOs and reverberating loops all seem to promote in a cooperative manner complex spike rhythmicity at a time scale of

about 200 ms. We found that not only the state of the inferior olivary oscillations determines which inputs are transmitted, but that these inputs also determine the state of the oscillations. Thus, inputs from both the cerebellum and the cerebrum determine the behavior of the inferior olive on a cycle-by-cycle basis. A circuit-wide understanding of cerebellar dynamics would open a novel pathway to explore the dynamic cerebellar gating by other brain regions.

A ratchet rather than a metronome

Well-coordinated movement sequences are not timed rigidly; they must be enacted flexibly and contextually. In order to catch a ball, or a prey, or to perform any other appropriately timed movement, it is essential to finely tune the duration of multiple coordinated output systems, for which knowledge of the phase of movement is necessary. An inferior olive that responds contextually to time varying input by advancing and delaying cycles does not act as a rigid clock or metronome, but more contextually, as a ratchet-pole system, where the phase of the ratchet would reflect an applied torque for a short duration. The ability to elongate or shorten a movement contextually can be subserved more aptly by an olive whose periods are continuously modulated to reflect delays or advancements in a phasic movement than regularly timed signals. The properties we have encountered in this study are consistent with a 'ratchet-like' function for the inferior olive, which integrates time-varying stimulus in a phase dependent manner, and 'clicks' as a function of the system's state. According to this view, the inferior olive responds to all input (sensory and otherwise), by producing phase changes that are informative about the recent history of input, either externally or internally generated.

METHODS

Animals

Experiments were performed on 16 adult (9 males and 7 females of 25 ± 14 weeks old) homozygous Gjd2^{tm1Kwi} (Gjd2 KO) mice which were compared to 15 wild-type littermates (8 males and 7 females of 26 ± 13 weeks old; means ± sd). The generation of these mice has been described previously (95). The mice received a magnetic pedestal that was attached to the skull above bregma using Optibond adhesive (Kerr Corporation, Orange, CA) and a craniotomy of the occipital bone above lobules crus 1 and crus 2. The surgery was performed under isoflurane anesthesia (2-4% V/V in O_2). Post-surgical pain was treated with 5 mg/kg carprofen ("Rimadyl", Pfizer, New York, NY) and 1 µg lidocaine (Braun, Meisingen, Germany). Mice were habituated during 2 daily sessions of 30-60 min. All experimental procedures were approved *a priori* by an independent animal ethical committee (DEC-Consult, Soest, The Netherlands) as required under Dutch law.

Electrophysiology

Extracellular recordings of Purkinje cells were made in the cerebellar lobules crus 1 and 2 of awake mice as described previously (22). Briefly, an 8x4 matrix of quartz-platinum electrodes (2-4 MΩ; Thomas Recording, Giessen, Germany) was used to make recordings that were amplified and digitized at 24 kHz using an RZ2 BioAmp processor (Tucker-Davis Technologies, Alachua, FL). The signals were analyzed offline with SpikeTrain (Neurasmus, Rotterdam, The Netherlands) using a digital band-pass filter (30-6,000 Hz). Complex spikes were recognized based on their waveform consisting of an initial spike followed by one or more spikelets. A recording was accepted as that of a single Purkinje cell when a discernible pause of at least 8 ms in simple spike firing followed the complex spikes and when the complex spikes were of similar shape and amplitude throughout the recording.

Sensory stimulation was applied as air puffs of 20 psi and 25 ms duration directed at the whisker pad ipsilateral to the side of recording. The stimuli were given in trains of 100 or 360 pulses either at regular or alternating intervals. During a recording, trains with different stimulus intervals were played in a random sequence.

Complex spike pattern analysis

Of each Purkinje cell we computed the probability density function (PDF) of both its complex spike autocorrelogram and its distribution of intervals between consecutive complex spikes (inter-complex spike intervals (ICSIs)). PDFs were calculated with an Epanechnikov kernel with a width of 10 ms. In order to exclude stimulus-induced alterations in complex spike firing, complex spikes detected between 20 and 200 ms after a stimulus were omitted from this analysis. PDFs were calculated from 0 up till 500 ms. The peak in the ICSI PDF was considered as the "preferred ICSI interval" and its strength was expressed as the Z-score by dividing the peak value by the standard deviation of the PDF. To avoid having Purkinje cell recordings with relatively low preference for specific ICSI intervals to distort our analysis we wanted to specifically also look at the Purkinje cells with a high Z-scores. Therefore, we grouped Purkinje cells into high and low level Z-scores, using a threshold of 3.

Air-puff stimulations frequently triggered double complex spike response peaks, suggestive of an underlying inferior olivary oscillation. For further analysis of the conditional responses, an estimate of the putative inferior olivary frequency was derived from the interval between these two response peaks. First, it was established for each Purkinje cell whether two peaks were present in the PSTH. To this end, we set a threshold for each of these two peaks. For the first peak, this was calculated by reshuffling the ICSIs over the recording followed by calculating a stimulus-triggered pseudo-PSTH, repeating this procedure 10,000 times and selecting the 99% upper-bound. We considered the first response peak to be significant if it crossed the upper-bound uninterruptedly for at least 10 ms. Since the second response peak typically is much smaller than the first one, we calculated a new threshold for the second peak by excluding the time-window for the first response peak. This window was set from the time of the stimulus until where the response probability drops to the average response frequency, the response frequency as expected if stimuli do not trigger complex spikes, following the significant 'first' responsive peak. In 5 out of 98 Purkinje cells, the PDF of the response rate between clear peaks remained above the average response rate, in which case we used the time point where the amplitude drop in the PDF was more than twice the difference between upper bound and average response probability. The rest of the bootstrap method was identical to that for the first response peak. Only peaks up to 0.5 s after the stimulus were included in the population analysis.

Prediction of response probability based on inferred olivary oscillation frequency

In order to test whether the phase of the inferior olivary oscillations affected the complex spike response probability, we compared the complex spike intervals over an air-puff for each stimulus that triggered a complex spike. To this end, we analyzed the recordings of 25 Purkinje cells (10 WT and 15 Gjd2 KO) that were measured previously in crus 1 and crus 2 of awake, adult mice. We included only Purkinje cells that displayed clear oscillatory complex spike firing indicated by the display of a secondary complex spike response peak, as evaluated according to the bootstrap method described above, and/or significant peaks in the ICSI histogram. Only stable recordings covering at least 500 stimuli at frequencies below 1 Hz were considered for this analysis.

For each recording we compared two idealized statistical models of the observed ICSI distributions: an oscillatory model showing phase dependent spiking and stable olivary oscillation frequencies and a uniform model lacking phase-dependencies. For the oscillatory model, we created complex spike probability functions for the pre-stimulus interval (-300 to 0 ms) based on the oscillatory period established either for the ICSI distribution or from the interval between the two complex spike response peaks. We fitted a sine wave with the observed frequency, having its peak at the moment of the first complex spike in the stimulus response window (20-200 ms after the air puff) and derived spike probability levels during the pre-stimulus interval from these fits, with the trough representing zero probability. Frequency and amplitude of every cycle were kept constant for the whole recording. In the uniform model, we calculated the pre-stimulus spiking probability with a uniform distribution based on the complex spike frequency of each Purkinje cell. We did include a refractory period, being the shortest ICSI observed for each recording, to reflect the inability of consecutive complex spikes to occur with a very short time interval. Refractory periods were comparable between mutants and wild types; 49 ± 15 ms for Gjd2 KO cells and 50 ± 20 ms for WT cells. Subsequently, we constructed compound fits consisting of linear summations of the two models. One extreme was the oscillatory model and the other the uniform model and we considered nine intermediate combinations (e.g., 0.3 x the oscillatory model + 0.7 x the uniform model). Every compound fit was run for 10,000 times. The goodness of fit was computed as the absolute differences of every single run of the model with the actual ICSI distribution.

Biophysically plausible IO model

The model networks used here are comprised of a topographical grid of 200 coupled cells, in a 10x10x2 arrangement. The single cells in the network are connected to an average of 8 neighboring cells with a maximum radius distance of two cells (reflecting anatomical constraints). Each cell within these networks was modelled according to the single cell model described in (40), which is an elaboration on a previous model (58). Briefly, the model includes three compartments (soma, dendrite, axon hillock) with differential distributions of conductances. The main ionic conductances responsible for the oscillation are the T-type Ca^{2+} and the Ca^{2+}-activated K^{+} (SK) channels present in the dendritic compartment. The crucial parameters governing the emergence of subthreshold oscillations are randomized, reflecting the experimental facts that about one third of the cells oscillate endemically (*in vivo*) with intrinsic variations in oscillatory frequencies (37). The behavior of the STO of the model cells in our network as a function of their parameters, for models with and without gap junctions, are included in Fig. 9 – Fig. supplement 1).

Network inputs

Two inputs are given to the model, one emulating the sensory input from whisker pad stimulation and the other representing a stimulus-independent background reflecting diverse excitatory and inhibitory inputs to the inferior olive. The latter consisted of a continuous stochastic process with known mean and standard deviation with a relaxation parameter following the Ornstein-Uhlenbeck process (82), succinctly described underneath.

Only one subset of cells in the center of the network (40% of the cells in a mask spanning a radius of 3 cells from the center of the network) representing efferent arborization, receives the "sensory input", with "sensory" currents being delivered to the soma of modelled cells (g_sensory = 0.15 mS/cm^2). "Sensory input" was modeled according to O'Donnel et al. (96). The mask is represented in Fig. 10A.

The cells of the inferior olivary network most likely share input sources due to overlapping arborizations of efferent projections (97). To represent both shared and independent input, we have modeled the current source in each cell as having an independent process and a shared process, with a mix parameter (alpha) of 10% input correlation shared by all the cells in the network. This generates a coherent background oscillation in the cells of the network, which is exacerbated in the presence of gap junctions (S4 Fig.).

Ornstein-Uhlenbeck noise process

Ornstein-Uhlenbeck (OU) is a noise process that ensures that the mean current delivered is well behaved and that the integral of delivered current over time converges to a constant value (82). The OU current is a good approximation for synaptic inputs originating in a large number of uncorrelated sources, where synaptic events are generated randomly and each event decays with a given rate (τ). We use a recursive implementation according to the following recursive formula:

FORMULA 1: $\eta(t+1)=\eta(n,t)*\exp(-\delta/\tau)+(1/\tau)(\mu-\eta(t))+\sigma*\sqrt{\delta}*\xi$

Where $\eta(t+1)$ is the noise value at $t+1$. The noise process is parameterized by τ,σ,μ where τ represents the synaptic decay time constant, δ is the integration step time for our forward Euler integrator, σ is the standard deviation of the noise process and μ is its mean. The random draw from a Gaussian distribution at every time step is represented by r_i.

Neurons in the inferior olive receive broad arborizations, signifying correlations in input sources across neurons. In our model we represent that via a mixture of an independent process for each neuron and a shared process, common to all the neurons in the network, parameterized by a mixing parameter α:

FORMULA 2: $n_i(t)=\alpha*n_i+(1-\alpha)*n_{all}(t)$

Simulation results throughout the article come from simulations with noise use an α where neurons share 10% of their noise input, though the main results are robust to changes in this value.

Network Parameter Spaces

To examine the dependence of network dynamics on the characteristics of the incoming input, we computed the 200 neuron network sweeping a grid of the main input parameters (τ,σ,μ,α) of the Ornstein-Uhlenbeck noise process. The network response in terms of STO frequency, population firing rates, proportion of firing neurons was analyzed with respect to a grid of input parameters. For comparability of statistics and reproducibility of results, all results displayed in this article were obtained from a single random seed. We have tested the network with multiple seeds and the results are qualitatively indistinguishable.

The parameters of the Ornstein-Uhlenbeck process were tuned such that the network emulating the wildtype network (with gap junctions, WT) produced an average frequency of 1 Hz and more than 95% of the model cells fire at least once every 5 seconds (the parameter space for the network responses including STO, population firing rate and proportion of cells that fire within 3s is found in S4B Fig.). The parameters to achieve these criteria are dependent on the total leak through the gap junctions. There are multiple methods to compensate the absent leak in the gapless network. In the present case, the network without gap junctions has been tuned to produce the same firing frequency as the network with gaps by increasing the membrane leak currents from 0.010 to 0.013 mS/cm^2. This results in a similar excitability but slightly lower STO frequency in the "mutant". The average firing rate behavior of the network shows a linear relationship with the standard deviation of the OU process (S4 Fig.). For the present network with balanced connectivity and a single gap conductance of 0.04 mS/cm^2, the Ornstein-Uhlenbeck parameters are (τ,σ,μ,α) μ = -0.6 pA/cm^2, σ = 0.6 pA/cm^2 and τ = 20 ms. τ is a decay parameter that represents the synaptic decay times expected for olivary inputs, in this case chosen to emulate dendritic GABA according to Devor and Yarom (98).

Synchrony and Frequency Estimation

Both synchrony and instantaneous frequency were estimated on the basis of a novel phase transformation of the membrane potential, which is more robust than the standard Hilbert transform, and can produce a linear phase response to the non-linear shape of the subthreshold oscillations (99). This transformation improves the estimation of the momentary phase and compensates for the fact that ionic mechanisms have different rates. To that end we have used the DAMOCO toolbox (100). From the instantaneous phase, the instantaneous frequency is simply the inverse of the first order finite difference of phases. Synchrony across cells is estimated with the Kuramoto order parameter:

FORMULA 3: $K(t)=|1/N \sum_{i=1}^{N} e^{i(\Psi(t)-\phi_i(t))}|$

Where ϕ_i is the phase of each neuron, N is the number of neurons and Ψ is the phase average of all oscillators.

Post-Spike Phase Responses

To estimate the phase response curve of the stimulated neurons, first a "sensory stimulus" is delivered at a

phase known to produce an action potential (and resetting). The location of the first peak after stimulation is recorded. Subsequently, eight more simulations receive another stimulus, with same parameters as the resetting stimulus, but at different phases (with an interval of $2\pi/8$). The effect of that stimulation (delay or advance) on the next peak is recorded as a phase delta. Results are plotted in Fig. 11.

Acknowledgements

The authors wish to thank Ilja IJpelaar and Mandy Rutteman for technical support and Sungho Hong, Marcel De Jeu, Jornt De Gruijl, Michiel Ten Brinke, Marylka Uusisaari, Yosef Yarom, Ben Torben-Nielsen and Rodolfo Llinás for excellent discussions.

Funding statement

We thank the Dutch Organization for Medical Sciences (ZonMw; C.I.D.Z.), Life Sciences (ALW; C.I.D.Z.), the ERC-advanced and ERC-PoC of the European Community (C.I.D.Z; M.N.) for their financial support.

Competing interests

The authors declare that they do not have any competing financial interests.

Author contributions

Conceptualization: P.W., M.N., L.W.J.B. and C.I.D.Z.; Data acquisition: P.W., M.N., V.R., C.B.O., S.L., E.I., L.W.J.B.; Network Modeling: M.N.; Formal analysis: P.W., M.N., V.R., C.B.O., S.L., E.I., L.W.J.B., C.I.D.Z.; Funding acquisition: C.I.D.Z.; Investigation: P.W., M.N., V.R., C.B.O., L.W.J.B.; Methodology: P.W., M.N., L.W.J.B.; Project administration: P.W., M.N., C.I.D.Z.; Software: P.W., M.N.; Supervision: M.N., L.W.J.B., C.I.D.Z.; Visualization: P.W., M.N., L.W.J.B., C.I.D.Z.; Writing – Original draft preparation: P.W., M.N.; Writing – Review & Editing: M.N., L.W.J.B., C.I.D.Z..

References

1. Roth MJ, Synofzik M, Lindner A. The cerebellum optimizes perceptual predictions about external sensory events. Curr Biol. 2013;23(10):930-5.

2. Grube M, Cooper FE, Chinnery PF, Griffiths TD. Dissociation of duration-based and beat-based auditory timing in cerebellar degeneration. Proc Natl Acad Sci U S A. 2010;107(25):11597-601.

3. Ashe J, Bushara K. The olivo-cerebellar system as a neural clock. Advances in Experimental Medicine and Biology. 2014;829:155-65.

4. Braitenberg V. Is the cerebellar cortex a biological clock in the millisecond range? Prog Brain Res. 1967;25:334-46.

5. Keele SW, Ivry R. Does the cerebellum provide a common computation for diverse tasks? A timing hypothesis. Ann N Y Acad Sci. 1990;608:179-207.

6. Ivry RB, Spencer RM, Zelaznik HN, Diedrichsen J. The cerebellum and event timing. Ann N Y Acad Sci. 2002;978:302-17.

7. De Gruijl JR, Bosman LWJ, De Zeeuw CI, De Jeu MTG. Inferior olive: All ins and outs. In: Manto M, Schmahmann JD, Rossi F, Gruol DL, Koibuchi N, editors. Handbook of the Cerebellum and Cerebellar Disorders. 3. Dordrecht: Springer Netherlands; 2013. p. 1013-58.

8. Llinás R, Walton K, Hillman DE, Sotelo C. Inferior olive: its role in motor learing. Science. 1975;190(4220):1230-1.

9. Choi S, Yu E, Kim D, Urbano FJ, Makarenko V, Shin HS, et al. Subthreshold membrane potential oscillations in inferior olive neurons are dynamically regulated by P/Q- and T-type calcium channels: a study in mutant mice. J Physiol. 2010;588(Pt 16):3031-43.

10. Horn KM, Deep A, Gibson AR. Progressive limb ataxia following inferior olive lesions. J Physiol. 2013;591(22):5475-89.

11. Koeppen AH. The pathogenesis of spinocerebellar ataxia. Cerebellum. 2005;4(1):62-73.

12. De Gruijl JR, Hoogland TM, De Zeeuw CI. Behavioral correlates of complex spike synchrony in cerebellar microzones. J Neurosci. 2014;34(27):8937-44.

13. De Zeeuw CI, Hoebeek FE, Bosman LWJ, Schonewille M, Witter L, Koekkoek SK. Spatiotemporal firing patterns in the cerebellum. Nat Rev Neurosci. 2011;12(6):327-44.

14. Wang JJ, Kim JH, Ebner TJ. Climbing fiber afferent modulation during a visually guided, multi-joint arm movement in the monkey. Brain Res. 1987;410(2):323-9.

15. Kitazawa S, Kimura T, Yin PB. Cerebellar complex spikes encode both destinations and errors in arm movements. Nature. 1998;392(6675):494-7.

16. Yang Y, Lisberger SG. Purkinje-cell plasticity and cerebellar motor learning are graded by complex-spike duration. Nature. 2014;510(7506):529-32.

17. Ito M. Long-term depression. Annu Rev Neurosci. 2003;12:85-102.

18. Welsh JP, Lang EJ, Suglhara I, Llinas R. Dynamic organization of motor control within the olivocerebellar system. Nature. 1995;374(6521):453-7.

19. Ten Brinke MM, Boele HJ, Spanke JK, Potters JW, Kornysheva K, Wulff P, et al. Evolving models of Pavlovian conditioning: cerebellar cortical dynamics in awake behaving mice. Cell Rep. 2015;13(9):1977-88.

20. Ten Brinke MM, Heiney S, Wang X, Proietti-Onori M, Boele HJ, Bakermans J, et al. Dynamic modulation of activity in cerebellar nuclei neurons during pavlovian eyeblink conditioning in mice. Elife. 2017;6.

21. Watson TC, Jones MW, Apps R. Electrophysiological mapping of novel prefrontal - cerebellar pathways. Front Integr Neurosci. 2009;3:18.

22. Bosman LWJ, Koekkoek SKE, Shapiro J, Rijken BFM, Zandstra F, van der Ende B, et al. Encoding of whisker input by cerebellar Purkinje cells. J Physiol. 2010;588(19):3757-83.

23. Gao Z, Davis C, Thomas AM, Economo MN, Abrego AM, Svoboda K, et al. A cortico-cerebellar loop for motor planning. Nature. in press.

24. Van Der Giessen RS, Koekkoek SK, van Dorp S, De Gruijl JR, Cupido A, Khosrovani S, et al. Role of olivary electrical coupling in cerebellar motor learning. Neuron. 2008;58(4):599-612.

25. Sotelo C, Llinás R, Baker R. Structural study of inferior olivary nucleus of the cat: morphological correlates of electrotonic coupling. J Neurophysiol. 1974;37(3):541-59.

26. Ruigrok TJH, de Zeeuw CI, van der Burg J, Voogd J. Intracellular labeling of neurons in the medial accessory olive of the cat: I. Physiology and light microscopy. J Comp Neurol. 1990;300(4):462-77.

27. De Zeeuw CI, Hertzberg EL, Mugnaini E. The dendritic lamellar body: a new neuronal organelle putatively associated with dendrodendritic gap junctions. J Neurosci. 1995;15(2):1587-604.

28. Llinás R, Yarom Y. Electrophysiology of mammalian inferior olivary neurones *in vitro*. Different types of voltage-dependent ionic conductances. J Physiol. 1981;315:549-67.

29. Yarom Y, Llinás R. Long-term modifiability of anomalous and delayed rectification in guinea pig inferior olivary neurons. J Neurosci. 1987;7(4):1166-77.

30. Gutnick MJ, Yarom Y. Low threshold calcium spikes, intrinsic neuronal oscillation and rhythm generation in the CNS. J Neurosci Methods. 1989;28(1-2):93-9.

31. Yarom Y. Rhythmogenesis in a hybrid system--interconnecting an olivary neuron to an analog network of coupled oscillators. Neuroscience. 1991;44(2):263-75.

32. Lampl I, Yarom Y. Subthreshold oscillations of the membrane potential: a functional synchronizing and timing device. J Neurophysiol. 1993;70(5):2181-6.

33. Lampl I, Yarom Y. Subthreshold oscillations and resonant behavior: two manifestations of the same mechanism. Neuroscience. 1997;78(2):325-41.

34. Manor Y, Rinzel J, Segev I, Yarom Y. Low-amplitude oscillations in the inferior olive: a model based on electrical coupling of neurons with heterogeneous channel densities. J Neurophysiol. 1997;77(5):2736-52.

35. Llinás R, Yarom Y. Oscillatory properties of guinea-pig inferior olivary neurones and their pharmacological modulation: an in vitro study. J Physiol. 1986;376:163-82.

36. Bazzigaluppi P, De Gruijl JR, van der Giessen RS, Khosrovani S, De Zeeuw CI, de Jeu MTG. Olivary subthreshold oscillations and burst activity revisited. Front Neural Circuits. 2012;6:91.

37. Khosrovani S, Van Der Giessen RS, De Zeeuw CI, De Jeu MTG. *In vivo* mouse inferior olive neurons exhibit heterogeneous subthreshold oscillations and spiking patterns. Proc Natl Acad Sci U S A. 2007;104(40):15911-6.

38. Leznik E, Llinás R. Role of gap junctions in synchronized neuronal oscillations in the inferior olive. J Neurophysiol. 2005;94(4):2447-56.

39. Mathy A, Clark BA, Häusser M. Synaptically induced long-term modulation of electrical coupling in the inferior olive. Neuron. 2014;81(6):1290-6.

40. De Gruijl JR, Bazzigaluppi P, de Jeu MTG, De Zeeuw CI. Climbing fiber burst size and olivary sub-threshold oscillations in a network setting. PLoS Comput Biol. 2012;8(12):e1002814.

41. Blenkinsop TA, Lang EJ. Block of inferior olive gap junctional coupling decreases Purkinje cell complex spike synchrony and rhythmicity. J Neurosci. 2006;26(6):1739-48.

42. Wylie DR, De Zeeuw CI, Simpson JI. Temporal relations of the complex spike activity of Purkinje cell pairs in the vestibulocerebellum of rabbits. J Neurosci. 1995;15(4):2875-87.

43. Bell CC, Kawasaki T. Relations among climbing fiber responses of nearby Purkinje Cells. J Neurophysiol. 1972;35(2):155-69.

44. Lang EJ, Sugihara I, Welsh JP, Llinás R. Patterns of spontaneous purkinje cell complex spike activity in the awake rat. J Neurosci. 1999;19(7):2728-39.

45. Keating JG, Thach WT. Nonclock behavior of inferior olive neurons: interspike interval of Purkinje cell complex spike discharge in the awake behaving monkey is random. J Neurophysiol. 1995;73(4):1329-40.

46. Hakimian S, Norris SA, Greger B, Keating JG, Anderson CH, Thach WT. Time and frequency characteristics of Purkinje cell complex spikes in the awake monkey performing a non-periodic task. J Neurophysiol. 2008.

47. Kubo R, Aiba A, Hashimoto K. The anatomical pathway from the mesodiencephalic junction to the inferior olive relays perioral sensory signals to the cerebellum in the mouse. J Physiol. 2018.

48. De Zeeuw CI, Simpson JI, Hoogenraad CC, Galjart N, Koekkoek SKE, Ruigrok TJH. Microcircuitry and function of the inferior olive. Trends Neurosci. 1998;21(9):391-400.

49. De Zeeuw CI, Holstege JC, Calkoen F, Ruigrok TJH, Voogd J. A new combination of WGA-HRP anterograde tracing and GABA immunocytochemistry applied to afferents of the cat inferior olive at the ultrastructural level. Brain Res. 1988;447(2):369-75.

50. Nelson BJ, Mugnaini E. The rat inferior olive as seen with immunostaining for glutamate decarboxylase. Anat Embryol (Berl). 1988;179(2):109-27.

51. Walberg F, Ottersen OP. Demonstration of GABA immunoreactive cells in the inferior olive of baboons (*Papio papio* and *Papio anubis*). Neurosci Lett. 1989;101(2):149-55.

52. Bloedel JR, Ebner TJ. Rhythmic discharge of climbing fibre afferents in response to natural peripheral stimuli in the cat. J Physiol. 1984;352:129-46.

53. Kazantsev VB, Nekorkin VI, Makarenko VI, Llinás R. Self-referential phase reset based on inferior olive oscillator dynamics. Proc Natl Acad Sci U S A. 2004;101(52):18183-8.

54. Llinás R, Baker R, Sotelo C. Electrotonic coupling between neurons in cat inferior olive. J Neurophysiol. 1974;37(3):560-71.

1009 55. Placantonakis DG, Bukovsky AA, Zeng XH, Kiem HP, Welsh JP. Fundamental role of inferior olive
1010 connexin 36 in muscle coherence during tremor. Proc Natl Acad Sci U S A. 2004;101(18):7164-9.
1011 56. De Zeeuw CI, Chorev E, Devor A, Manor Y, Van Der Giessen RS, De Jeu MT, et al. Deformation of
1012 network connectivity in the inferior olive of connexin 36-deficient mice is compensated by morphological and
1013 electrophysiological changes at the single neuron level. J Neurosci. 2003;23(11):4700-11.
1014 57. Latorre R, Aguirre C, Rabinovich MI, Varona P. Transient dynamics and rhythm coordination of
1015 inferior olive spatio-temporal patterns. Front Neural Circuits. 2013;7:138.
1016 58. Schweighofer N, Doya K, Kawato M. Electrophysiological properties of inferior olive neurons: A
1017 compartmental model. J Neurophysiol. 1999;82(2):804-17.
1018 59. Yu Y, Fu Y, Watson C. The inferior olive of the C57BL/6J mouse: a chemoarchitectonic study. Anat Rec
1019 (Hoboken). 2014;297(2):289-300.
1020 60. Lefler Y, Yarom Y, Uusisaari MY. Cerebellar inhibitory input to the inferior olive decreases electrical
1021 coupling and blocks subthreshold oscillations. Neuron. 2014;81(6):1389-400.
1022 61. Turecek J, Yuen GS, Han VZ, Zeng XH, Beyer KU, Welsh JP. NMDA receptor activation strengthens
1023 weak electrical coupling in mammalian brain. Neuron. 2014;81(6):1375-88.
1024 62. Zhou H, Lin Z, Voges K, Ju C, Gao Z, Bosman LWJ, et al. Cerebellar modules operate at different
1025 frequencies. eLIFE. 2014;3:e02536.
1026 63. Lefler Y, Torben-Nielsen B, Yarom Y. Oscillatory activity, phase differences, and phase resetting in
1027 the inferior olivary nucleus. Front Syst Neurosci. 2013;7:22.
1028 64. Coesmans M, Weber JT, De Zeeuw CI, Hansel C. Bidirectional parallel fiber plasticity in the cerebellum
1029 under climbing fiber control. Neuron. 2004;44(4):691-700.
1030 65. Badura A, Schonewille M, Voges K, Galliano E, Renier N, Gao Z, et al. Climbing fiber input shapes
1031 reciprocity of Purkinje cell firing. Neuron. 2013;78(4):700-13.
1032 66. Mathy A, Ho SSN, Davie JT, Duguid IC, Clark BA, Häusser M. Encoding of oscillations by axonal bursts
1033 in inferior olive neurons. Neuron. 2009;62(3):388-99.
1034 67. Ebner TJ, Bloedel JR. Climbing fiber action on the responsiveness of Purkinje cells to parallel fiber
1035 inputs. Brain Res. 1984;309(1):182-6.
1036 68. Simpson JI, Wylie DR, De Zeeuw CI. On climbing fiber signals and their consequence(s). Behav Brain
1037 Sci. 1996;19(2):384-98.

69. Llinás R, Volkind RA. The olivo-cerebellar system: functional properties as revealed by harmaline-induced tremor. Exp Brain Res. 1973;18(1):69-87.

70. Llinás RR. Inferior olive oscillation as the temporal basis for motricity and oscillatory reset as the basis for motor error correction. Neuroscience. 2009;162(3):797-804.

71. Alvarez-Icaza R, Boahen K. Inferior olive mirrors joint dynamics to implement an inverse controller. Biol Cybern. 2012;106(8-9):429-39.

72. Armstrong DM, Edgley SA, Lidierth M. Complex spikes in Purkinje cells of the paravermal part of the anterior lobe of the cat cerebellum during locomotion. J Physiol. 1988;400:405-14.

73. Romano V, De Propris L, Bosman LWJ, Warnaar P, Ten Brinke MM, Lindeman S, et al. Adaptation of whisker movements requires cerebellar potentiation. bioRxiv. 2018:335489.

74. Ju C, Bosman LWJ, Hoogland TM, Velauthapillai A, Murugesan P, Warnaar P, et al. Neurons of the inferior olive respond to broad classes of sensory input while subject to homeostatic control. bioRxiv. 2018:379149.

75. Zhang Y, Zhang Z, Xiao S, Tien J, Le S, Le T, et al. Inferior olivary TMEM16B mediates cerebellar motor learning. Neuron. 2017;95(5):1103-11 e4.

76. Chaumont J, Guyon N, Valera AM, Dugué GP, Popa D, Marcaggi P, et al. Clusters of cerebellar Purkinje cells control their afferent climbing fiber discharge. Proc Natl Acad Sci U S A. 2013;110(40):16223-8.

77. Witter L, Canto CB, Hoogland TM, de Gruijl JR, De Zeeuw CI. Strength and timing of motor responses mediated by rebound firing in the cerebellar nuclei after Purkinje cell activation. Front Neural Circuits. 2013;7:133.

78. Bal T, McCormick DA. Synchronized oscillations in the inferior olive are controlled by the hyperpolarization-activated cation current I(h). J Neurophysiol. 1997;77(6):3145-56.

79. Best AR, Regehr WG. Inhibitory regulation of electrically coupled neurons in the inferior olive is mediated by asynchronous release of GABA. Neuron. 2009;62(4):555-65.

80. Wiklund L, Björklund A, Sjölund B. The indolaminergic innervation of the inferior olive. 1. Convergence with the direct spinal afferents in the areas projecting to the cerebellar anterior lobe. Brain Res. 1977;131(1):1-21.

81. Leznik E, Makarenko V, Llinás R. Electrotonically mediated oscillatory patterns in neuronal ensembles: An *in vitro* voltage-dependent dye-imaging study in the inferior olive. J Neurosci. 2002;22(7):2804-15.

82. Uhlenbeck GE, Ornstein LS. On the theory of Brownian motion. Phys Rev. 1930;36(5):823-41.

83. Marshall SP, van der Giessen RS, de Zeeuw CI, Lang EJ. Altered olivocerebellar activity patterns in the connexin36 knockout mouse. Cerebellum. 2007;6(4):287-99.

84. Winfree AT. The geometry of biological time. 1 ed: Springer Science; 1980.

85. Ozden I, Sullivan MR, Lee HM, Wang SSH. Reliable coding emerges from coactivation of climbing fibers in microbands of cerebellar Purkinje neurons. J Neurosci. 2009;29(34):10463-73.

86. Schultz SR, Kitamura K, Post-Uiterweer A, Krupic J, Häusser M. Spatial pattern coding of sensory information by climbing fiber-evoked calcium signals in networks of neighboring cerebellar Purkinje cells. J Neurosci. 2009;29(25):8005-15.

87. White JJ, Sillitoe RV. Genetic silencing of olivocerebellar synapses causes dystonia-like behaviour in mice. Nat Commun. 2017;8:14912.

88. Ruigrok TJH, Voogd J. Cerebellar influence on olivary excitability in the cat. Eur J Neurosci. 1995;7(4):679-93.

89. Szentágothai J, Rajkovits K. Über den Ursprung der Kletterfasern des Kleinhirns. Z Anat Entwicklungsgesch. 1959;121(2):130-41.

90. Hoebeek FE, Witter L, Ruigrok TJH, De Zeeuw CI. Differential olivo-cerebellar cortical control of rebound activity in the cerebellar nuclei. Proc Natl Acad Sci U S A. 2010;107(18):8410-5.

91. Dykstra S, Engbers JDT, Bartoletti TM, Turner RW. Determinants of rebound burst responses in rat cerebellar nuclear neurons to physiological stimuli. J Physiol. 2016;594(4):985-1003.

92. Bengtsson F, Ekerot CF, Jörntell H. *In vivo* analysis of inhibitory synaptic inputs and rebounds in deep cerebellar nuclear neurons. PLoS One. 2011;6(4):e18822.

93. Rowland NC, Jaeger D. Responses to tactile stimulation in deep cerebellar nucleus neurons result from recurrent activation in multiple pathways. J Neurophysiol. 2008;99(2):704-17.

94. De Zeeuw CI, Ruigrok TJH, Schalekamp MPA, Boesten AJ, Voogd J. Ultrastructural study of the cat hypertrophic inferior olive following anterograde tracing, immunocytochemistry, and intracellular labeling. Eur J Morphol. 1990;28(2-4):240-55.

95. Güldenagel M, Ammermüller J, Feigenspan A, Teubner B, Degen J, Söhl G, et al. Visual transmission deficits in mice with targeted disruption of the gap junction gene connexin36. J Neurosci. 2001;21(16):6036-44.

96. O'Donnell C, Nolan MF, van Rossum MCW. Dendritic spine dynamics regulate the long-term stability of synaptic plasticity. J Neurosci. 2011;31(45):16142-56.

97. Scheibel ME, Scheibel AB. The inferior olive; a Golgi study. J Comp Neurol. 1955;102(1):77-131.

98. Devor A, Yarom Y. Electrotonic coupling in the inferior olivary nucleus revealed by simultaneous double patch recordings. J Neurophysiol. 2002;87(6):3048-58.

99. Kralemann B, Frühwirth M, Pikovsky A, Rosenblum M, Kenner T, Schaefer J, et al. *In vivo* cardiac phase response curve elucidates human respiratory heart rate variability. Nat Commun. 2013;4:2418.

100. Kralemann B, Cimponeriu L, Rosenblum M, Pikovsky A, Mrowka R. Phase dynamics of coupled oscillators reconstructed from data. Physical Review E. 2008;77(6 Pt 2):066205.

Supplementary information captions

Fig. S1 - Comparison of autocorrelogram with inter-complex spike interval histogram. The autocorrelogram of the same Purkinje cell as shown in Figure 3A (10 ms bins) convolved with a 5 ms kernel (red curve) compared to the convolved inter-complex spike interval (ICSI) histogram. The auto-correlogram includes also intervals between non-consecutive complex spikes. Consequently, on a short time scale, both auto-correlogram and ICSI histogram are identical, but they diverge at longer time scales.

Fig. S2. - No phase-dependent spiking probabilities observed in vivo. In addition to the 400 / 250 ms gallop stimuli (Figure 5) we also applied a 250 / 300 ms gallop with essentially the same results: absence of a clear preference for complex spike firing during one or the other stimulus interval.

Fig. S3 - No phase-dependent spiking probabilities observed in vivo (conditional analysis) (**A**) In order to test the impact of the presumed phase of the inferior olivary neurons in vivo, we applied a "gallop" stimulation pattern, alternating 250 ms and 400 ms intervals. Air puffs (vertical bars) were delivered to the whisker pad. Complex spikes were counted in response windows (RW) 20-200 ms post-stimulus. Response probabilities were compared between response windows in short and long intervals. For this analysis, which was based on the same data as presented in Figure 5A, we included only those response windows that followed a response window that contained at least one complex spike (blue lines). In the schematic drawing, this means that the response windows indicated with dashed lines were omitted from the analysis. This analysis resulted in very similar results as that using all response windows (Figure 5A) as summarized in Figure 5B. The Purkinje cells were sorted according to the same sequence as in Figure 5A. (**B**) The same for the experiments with the 250/300 ms gallop stimuli.

Fig. S4 - Behavior of model networks of identical cell composition as a function of the decay parameter of the Ornstein-Uhlenbeck process (tau) and the noise correlation (eta). Model networks have been computed using a systematic exploration of the parameter space using 56 instances of the network model. The contour plots indicate isolines for synchrony (A), frequency of subthreshold oscillations (STOs), population firing rate and proportion of active cells (B). The results presented in the main text come from a model network with parameters chosen such as to display STOs with mean of 9 Hz, a population rate of about 1 Hz and with more

than 70% of cells firing in three seconds (95% of cells fire within 10 s of simulation time). The position of this network in the contour plots is indicated with a red circle. In A, the thumbnails exemplify behaviors of extreme instances of the model network both as membrane potentials traces (top) and as heatmaps of the membrane potential (bottom). Arrows indicate parameter space coordinates of these examples. The decay of the Ornstein-Uhlenbeck process (tau) mostly impacts the firing rate of the model networks, while noise correlation (eta) has a direct effect on synchrony. (B) Gap junctions amplify the input correlation given to the neurons, while having a minor effect on other aspects of the network dynamics.

Fig. S5 - Contour plot indicating the average firing rate of networks as a function of the mean and standard deviation of the OU input. (A) Baseline input was chosen such that the cells of the model networks would produce approximately 1 Hz of spontaneous firing rate. The absence of gap junctional coupling in "mutant" model networks (B) leads to increased firing rate, which was compensated for by increasing the leak current of the membrane by 0.003 mS/cm^2 (data not shown).

Fig. S6 - Physiological properties of the individual model cells as a function of Ca^{2+} T-Type conductance the absence of "contextual input" in the presence (blue) and absence (red) of gap junctional coupling. The Ca^{2+} T type conductance is varied in the range of 0.5 to 1.1 mS/cm^2, resulting in a range of oscillatory properties of the individual model cells. The left axis in the panels of the main diagonal display cell counts for the histograms. The right axis besides the rightmost panel displays the indicated continuous variable. The set of non-oscillating (zero amplitude, zero frequency) cells constituted about 25% of the model network in the absence of gap junctions (red), were engaged in the oscillation when gaps were added to these cells (blue). In the absence of "contextual input" the distribution of frequencies had peaks at zero and sharply synchronizes at approximately in the absence of Ornstein-Uhlenbeck input.

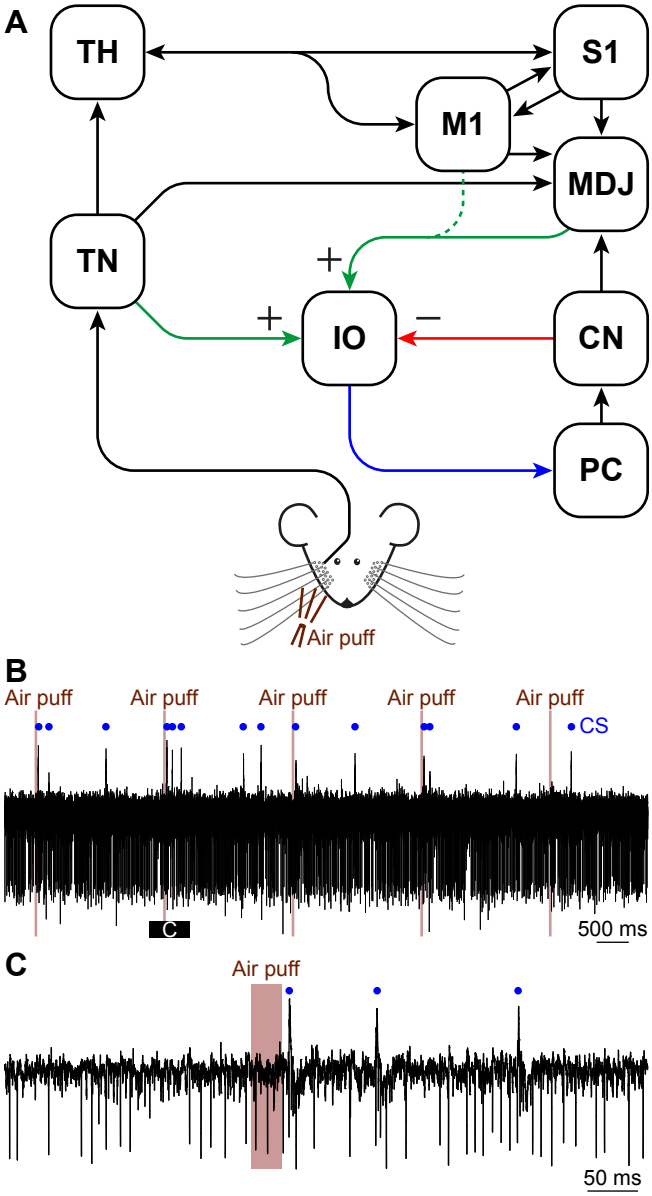

Fig. 1. Circuit involved in the production and modulation of complex spikes. (A) Simplified scheme of the inputs to the inferior olive (IO). Sensory input reaches the IO directly from the brainstem and spinal cord. In our study, we used facial whisker input that is relayed via the sensory trigeminal nuclei (TN). This input is considered the “sensory input” in our modeling studies. The IO also receives continuous inputs from other brain regions, which we modeled as the “contextual input”. The contextual input consists of excitatory input from the cerebral cortex (e.g., the motor (M1) and somatosensory cortex (S1)), either directly or relayed via the nuclei of the meso-diencephalic junction (MDJ), as well as of inhibitory input from the cerebellar nuclei (CN). The output of the IO is exclusively directed to the cerebellum and predominantly to the cerebellar Purkinje cells (PN). Obviously, the sensory input also affects the contextual input indirectly, via the strong pathway from the TN via the thalamus (TH) to the cerebral cortex. (B) Representative trace of Purkinje cell activity showing many simple spikes (as downward deflections) and occasional complex spikes (marked with a blue dot). A part of the trace is enlarged in panel (C). Recordings were made in awake mice.

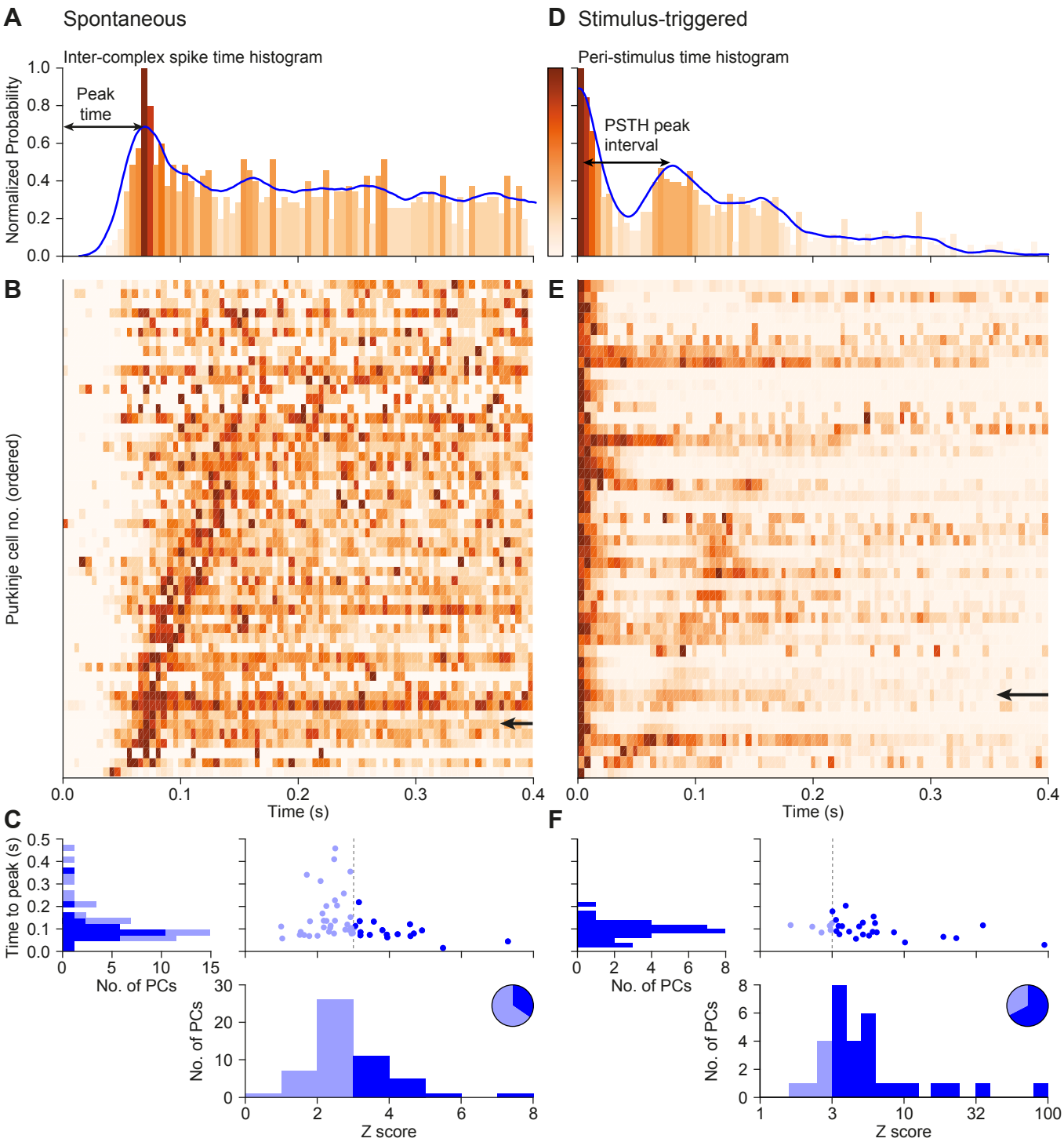

Fig. 2. Oscillatory dynamics in complex spike firing in vivo. (A) Representative inter-complex spike-interval (ICSI) histogram of spontaneous firing of a representative Purkinje cell, together with the convolved probability density function and after pruning the peak at 0 ms to improve visibility. The colors of the bins represent the normalized oscillation strength, which were used to create the heat maps of 52 Purkinje cells (B). The arrow indicates the cell taken as illustration in A. (C) The peak times of the ICSI distributions during spontaneous firing, as observed in B, against the Z-scores of these peaks. A Z-score <3 was taken as sign for the absence of rhythmicity. The pie diagram shows the fraction of Purkinje cells with rhythmic complex spike firing (dark blue area). (D)-(F) The same for whisker air puff stimulation-triggered complex spike firing as characterized by a peri-stimulus time histogram (PSTH).

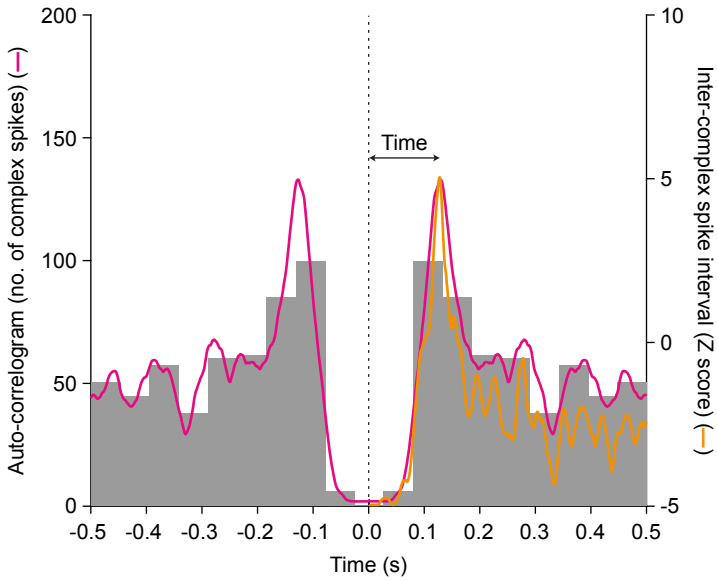

Fig. S1 - Comparison of autocorrelogram with inter-complex spike interval histogram. The autocorrelogram of the same Purkinje cell as shown in Figure 3A (10 ms bins) convolved with a 5 ms kernel (red curve) compared to the convolved inter-complex spike interval (ICSI) histogram. The auto-correlogram includes also intervals between non-consecutive complex spikes. Consequently, on a short time scale, both auto-correlogram and ICSI histogram are identical, but they diverge at longer time scales.

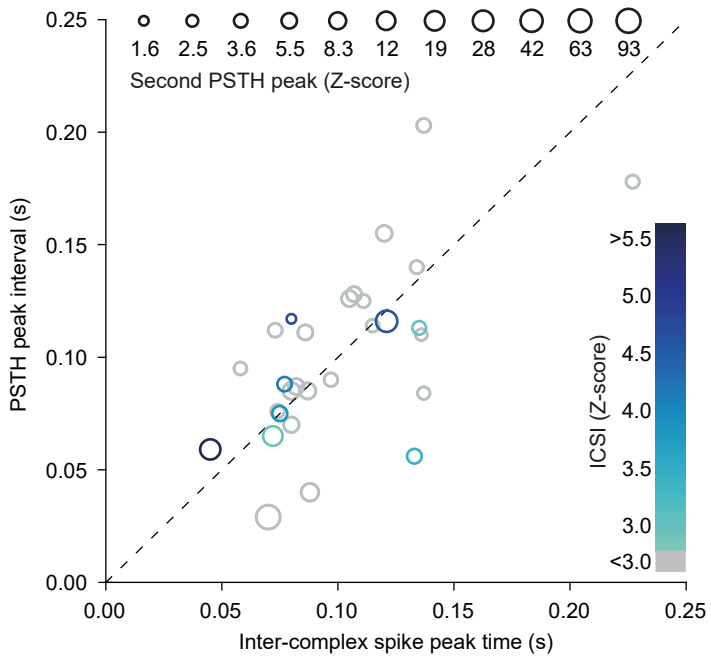

Fig. 3. Similarity between spontaneous and sensory-induced rhythmicity. Scatter plot of response peaks intervals versus ICSI peak intervals. Color and size of data points indicate height (in Z-score) of respectively the ICSI peak and the second response peak. Grey scatter-points indicate the data-points falling in the low Z-score (<3) group during spontaneous firing. Note that the colored symbols cluster around the identity line.

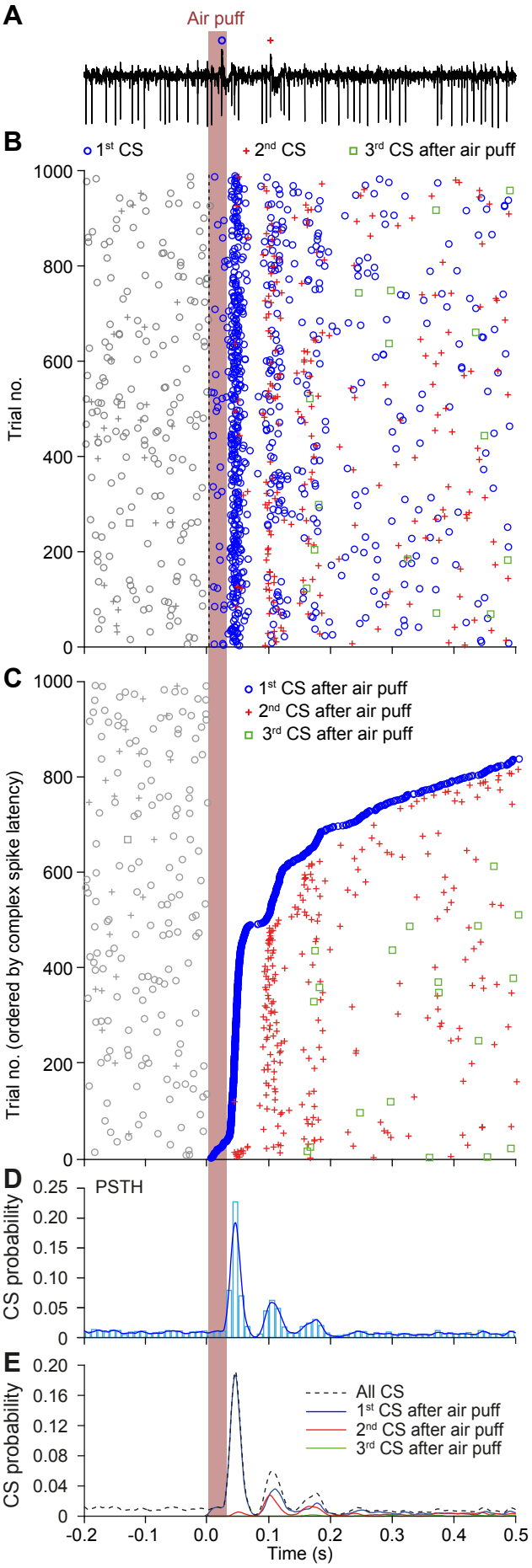

Fig. 4. Sensory stimulation can induce oscillatory complex spike firing in Purkinje cells of awake mice. (A) Whisker stimulation (Air puff) can trigger rhythmic complex spike (CS) firing in Purkinje cells of cerebellar lobules crus 1 and crus 2 of awake mice. This is illustrated by a representative extracellular recording. Two triggered CSs are marked according to their order following the stimulus. (cont. next page).

(B) Windows of opportunity for the occurrence of triggered complex spikes become apparent in a raster plot. (C) The same data, but now the trials are sorted by the latency of the first complex spike following the stimulus. Note that during trials during which no complex spike is fired during the first window of opportunity, the first complex spike after the stimulus often occurs in the second window of opportunity. (D) Peri-stimulus time histogram of complex spikes firing around a stimulus. The bin-width is 10 ms and convolved with a 5 ms kernel (see Methods). (E) The same peri-stimulus histogram as in D, but now the probabilities of the first, second and third complex spike after the stimulus are shown separately, highlighting the occurrence of windows of opportunity for stimulus-triggered complex spikes.

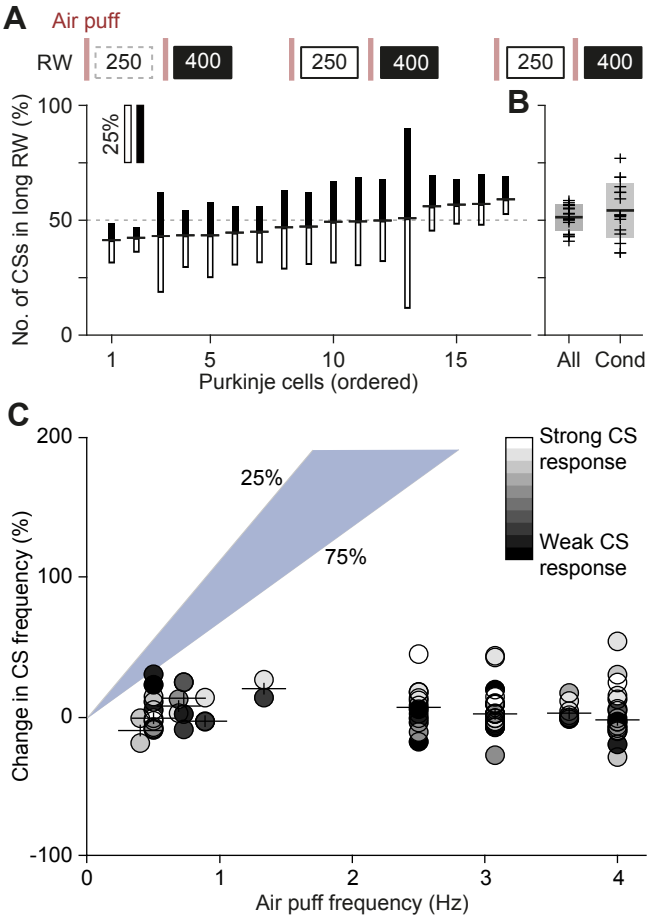

Fig. 5. No phase dependent spiking probabilities observed in in vivo. (A) In order to test the impact of the presumed phase of the inferior olivary neurons in vivo, we applied a “gallop” stimulation pattern, alternating short (250 ms) and long (400 ms) intervals. Air puffs (vertical bars) were delivered to the whisker pad. Complex spikes were counted in response windows (RW) 20-200 ms post-stimulus. Response probabilities were compared between response windows in short and long intervals. The first response window is not included in the analysis because it is not preceded by an air-puff interval. The ratio between number of complex spikes in short and long intervals for the entire population of cells were sorted on the fraction of complex spikes falling in the long response window (indicated as horizontal black lines). For each Purkinje cell the relative response probabilities for the long and short intervals are illustrated as the length of the filled and open bars, respectively. None of the Purkinje cells showed a significant difference in the response probability between the two intervals (all $p > 0.05$ on Fisher’s exact test). (B) This analysis was repeated, but now including only those response windows that followed a response window with at least one complex spike. This conditional approach (Cond) resulted in similar results as obtained from the analysis of all response windows (All). Shown are the 25 and 75 % quantiles and median per population. (C) If sensory stimulation triggers complex spikes, one would expect that a higher frequency of stimulation would lead to a higher frequency of complex spikes. However, such a relation was absent. For this analysis, we included only sensory-responsive Purkinje cells that crossed a bootstrap-derived 99% probability threshold. The gray scaling of the symbols indicates the response probability. Purkinje cells displaying a higher complex spike response rate had a slightly increased firing rate upon higher stimulus frequencies, but this was far from the expected increase (based upon a linear increase; the shaded area indicates the 25-75% probability range (see Methods)).

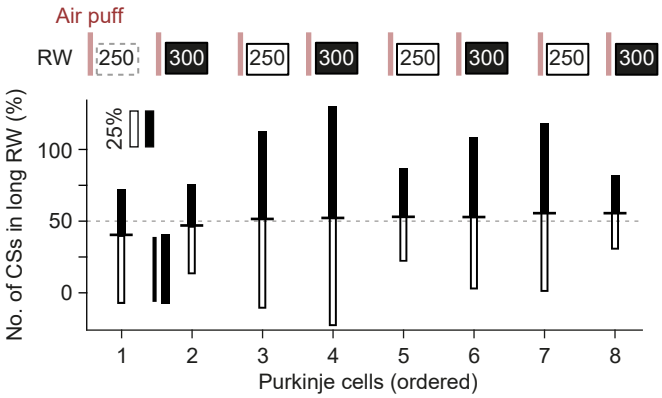

Fig. S2 - No phase-dependent spiking probabilities observed in vivo. In addition to the 400 / 250 ms gallop stimuli (Figure 5) we also applied a 250 / 300 ms gallop with essentially the same results: absence of a clear preference for complex spike firing during one or the other stimulus interval.

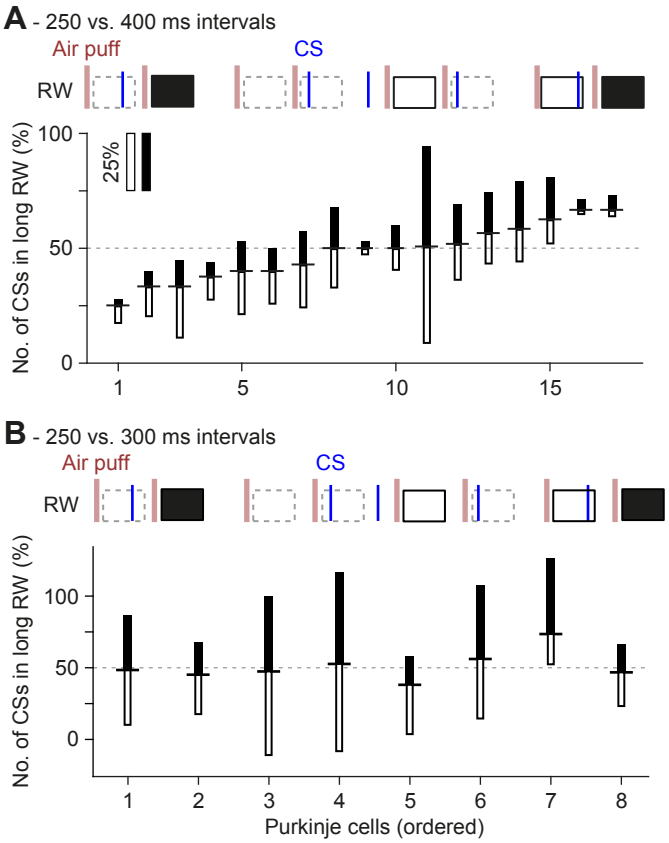

Fig. S3 - No phase-dependent spiking probabilities observed in vivo (conditional analysis) A. In order to test the impact of the presumed phase of the inferior olivary neurons in vivo, we applied a “gallop” stimulation pattern, alternating 250 ms and 400 ms intervals. Air puffs (vertical bars) were delivered to the whisker pad. Complex spikes were counted in response windows (RW) 20-200 ms post-stimulus. Response probabil- ities were compared between response windows in short and long intervals. For this analysis, which was based on the same data as presented in Figure 5A, we included only those response windows that followed a response window that contained at least one complex spike (blue lines). In the schematic drawing, this means that the response windows indicated with dashed lines were omitted from the analysis. This analysis resulted in very similar results as that using all response windows (Figure 5A) as summarized in Figure 5B. The Purkinje cells were sorted according to the same sequence as in Figure 5A. B. The same for the experiments with the 250/300 ms gallop stimuli (Fig. S3).

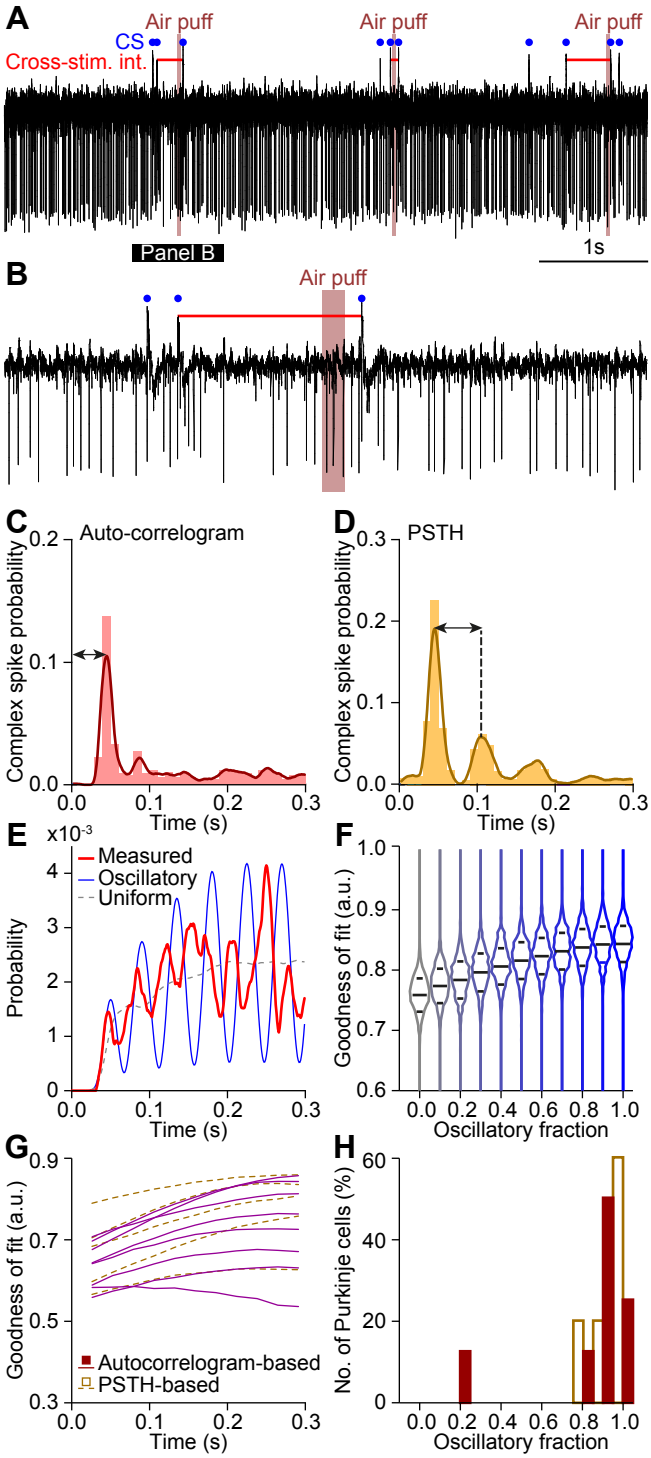

Fig. 6. Sensory stimulation leads to unconditional complex spike responses in vivo. (A) We quantified the impact of ongoing subthreshold oscillations on the occurrence and timing of CSs by comparing the cross-stimulus interval between the last complex spike before and the first complex spike after a sensory stimulus to the preferred firing frequency of each individual PN. This approach is illustrated by the analysis of a single, representative Purkinje cell: the data in A-E originate from the same cell. A representative trace is shown in (A) and enlarge in (B), showing the cross-stimulus interval as a horizontal red line. (C) For each Purkinje cell, we first established the preferred firing rates based upon the auto-correlogram (C) and the peri-stimulus time histogram (D; cf. Fig. 3). The histograms were convolved with an Epanechnikov kernel (see Methods). The intervals between the last complex spike before and the first complex spike after the stimulus for each trial yielded for each neuron a curve (red line). The observed probability density function was compared with calculated probability density functions based upon predicted firing based upon a uniform complex spike distribution (dotted line), an oscillatory complex spike distribution (blue line) and 9 intermediate models that were combinations of these two extremes with different relative weights (see Methods). (F) The distributions of the goodness-of-fit for each of the 11 models showed a clear bias towards the uniform model, refuting the impact of subthreshold oscillations on sensory-induced complex spike firing. Each model was run 1,000 times. The middle line indicates the average of all runs, the upper and lower lines, indicate 75 and 25% quantiles. (G) Distributions of the goodness-of-fit of all Purkinje cells that showed clear rhythmicity (see Methods) emphasized the bias towards the uniform firing model. (H) Histograms of the maxima in the distributions shown in G confirm that the impact of the subthreshold oscillations on sensory CS responses is minimal.

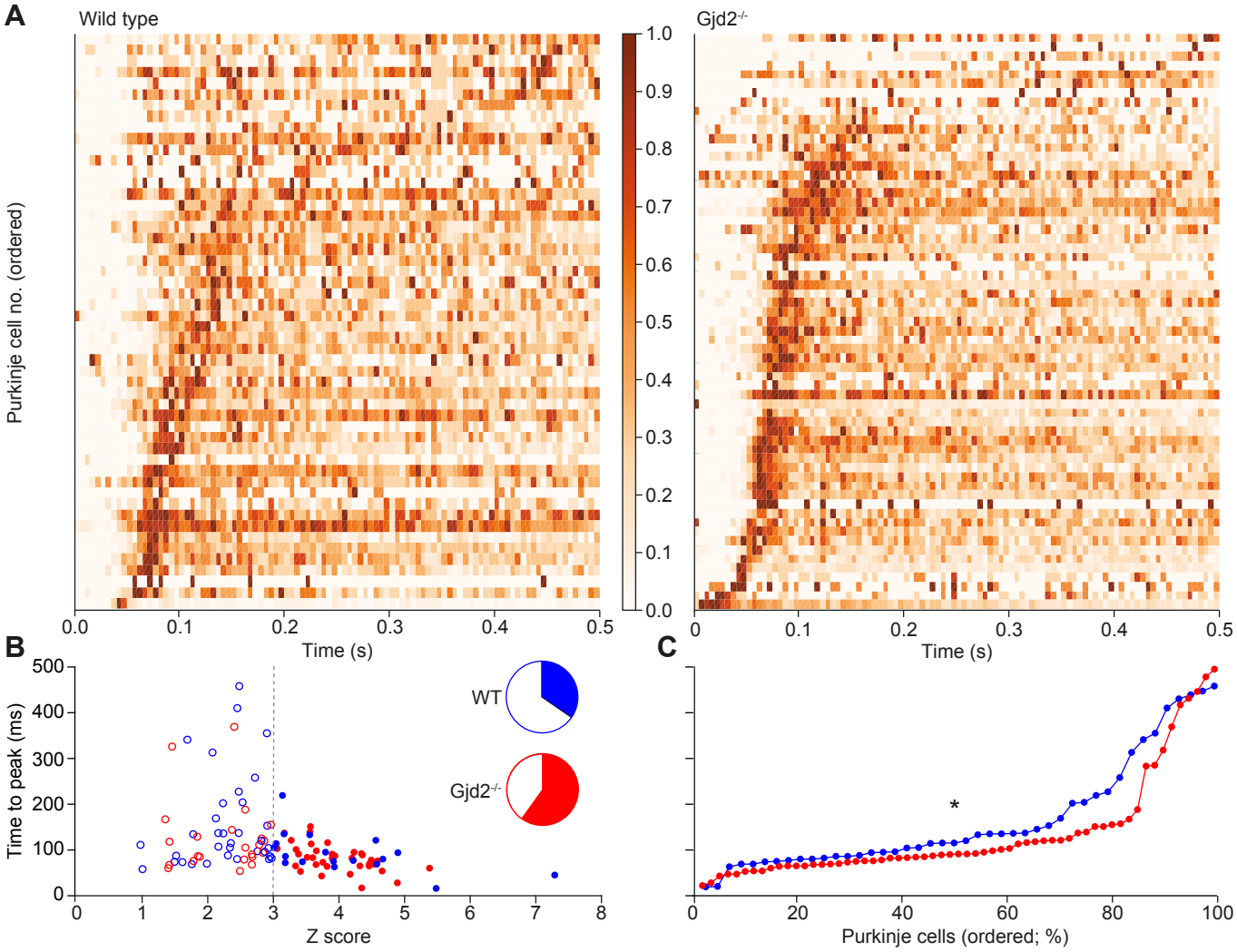

Fig. 7. Oscillatory dynamics in spontaneous firing in vivo in the presence and absence of gap junctions. (A) Color-coded inter-complex spike-interval (ICSI) histogram of spontaneous firing of 60 Gjd2-/- and 52 wild-type Purkinje cells. (B) The Gdj2-/- PN distribution shows higher Z-scores than the wild-type population, indicating a stronger rhythmicity during spontaneous firing in the absence of gap junctions ($p = 0.003$; Kolmogorov-Smirnov test). A Z-score <3 was taken as sign for the absence of rhythmicity – which occurred more often in the WT than in the Gjd2 KO PNs (colored fraction in the pie diagrams; $p = 0.005$; Fisher's exact test). In the absence of gap junctions, rhythmic firing was more stereotypical, as illustrated by less variation in the time to peak (C). Note that the left panel of A is a copy of Fig. 2B and presented here to facilitate comparison.

Figure 7

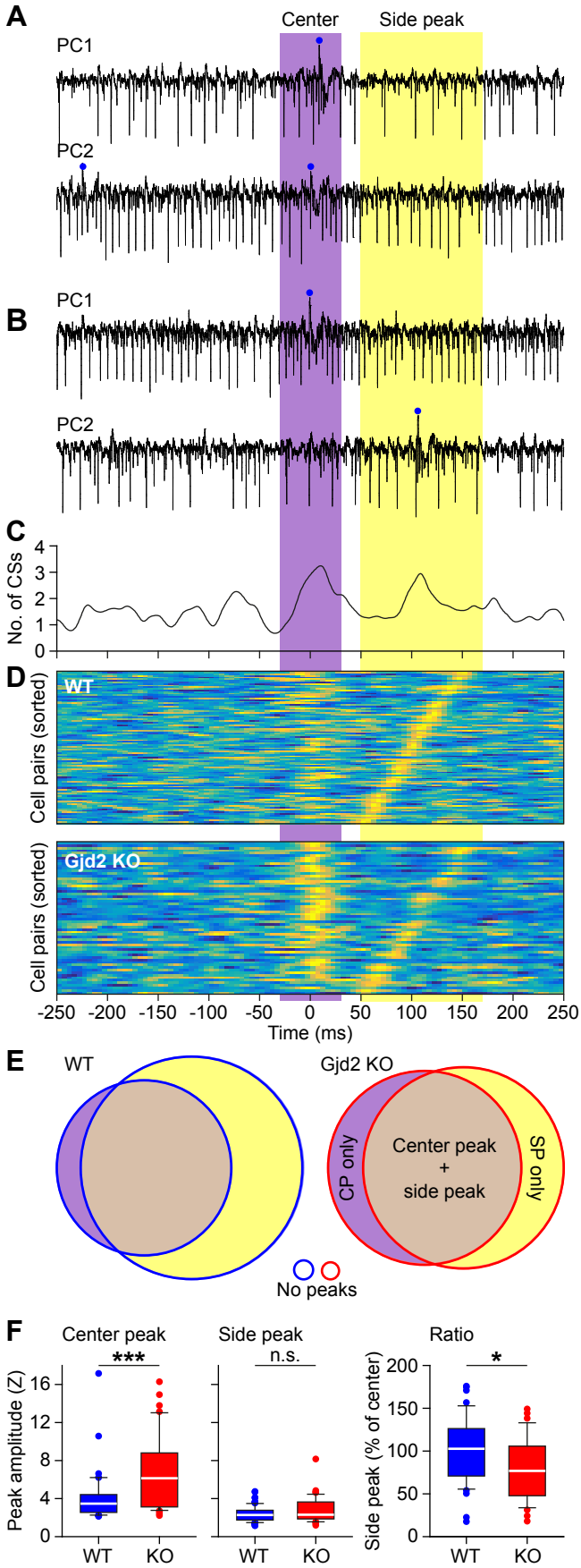

Fig. 8. Coherence of complex spike firing of Purkinje cells over time. Two Purkinje cells recorded simultaneously in a wild-type (WT) mouse during spontaneous activity, showing an epoch with near-synchronous complex spike firing with both spikes in the center-time interval (A), or another epoch at which the same cells fired temporally further apart with one complex spike in the center-time and another one in the side-peak interval (B), leading to a double-peaked cross-correlogram for this cell pair (C). (D) Heat map representations of cross-correlograms between simultaneously recorded Purkinje cells in WTs and Gjd2 KOs. Note the stronger impact of the center peak in Gjd2 KO mice compared to WT mice. However, the side peak, the latency of which was used to order the cell pairs, is stronger in WT pairs. The side peak can be regarded as a “network echo”. (E) Venn diagrams showing the relative occurrence of center and side peaks in the presence and absence of gap junctions. (F) In the absence of gap junctions, the center peak, but not the side peak, was stronger (Left and middle panel). Likewise, the normalized ratio of the side peak vs that of the center peak was lower in the Gjd2 KO mice (right panel). * $p < 0.05$; *** $p < 0.001$ (t test)

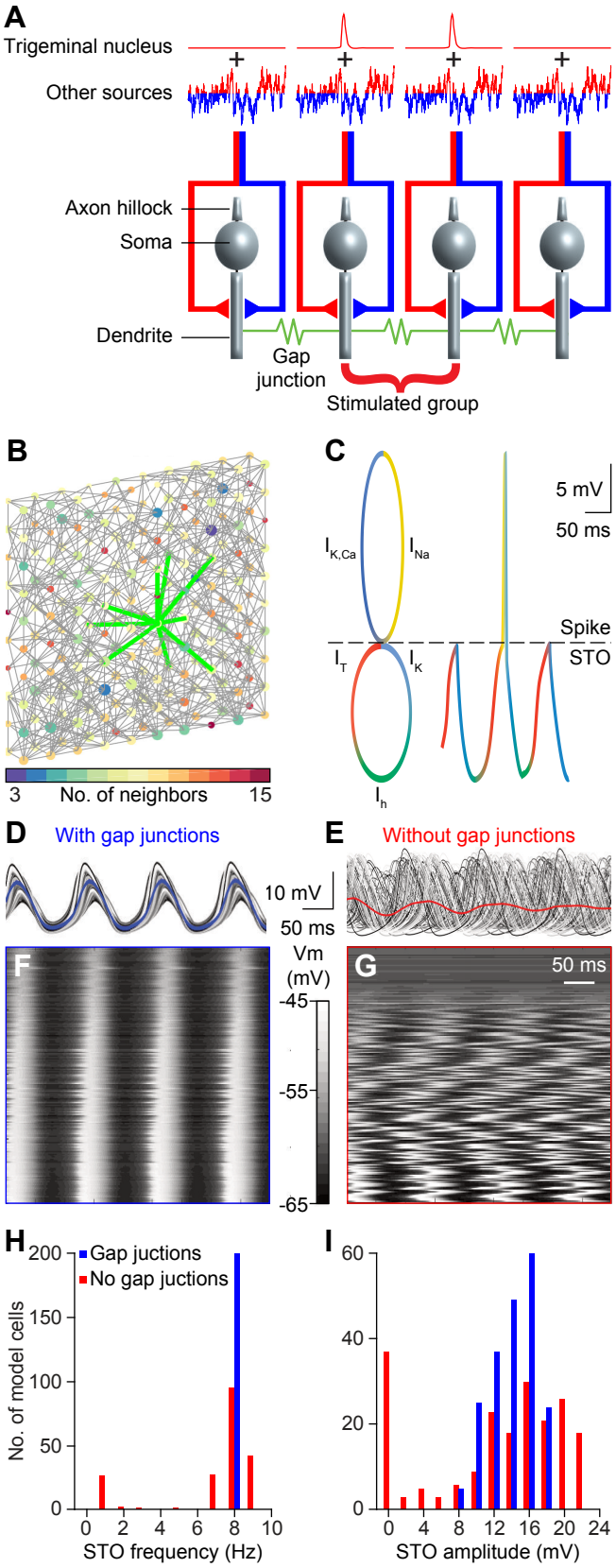

Fig. 9. A biophysically plausible network model of the inferior olive. (A) To study the relative impact of the different components of the inferior olive we employed a biologically realistic network consisting of 200 model neurons. The model neurons received input from two sources: a coupled, phasic input mimicking sensory input. The "sensory input" reaches a subset of neurons synchronously and with equal strength. The "sensory input" is complemented with a continuous input that is a mixture of excitatory and inhibitory synapses representing feedback signals from different sources, providing a functional context to the inferior olive. This "contextual input" is modeled as an Ornstein-Uhlenbeck (OU) noise process delivered to all neurons in the model network with a 10% correlation over time (see Methods). As in the biological counterpart, the model neurons are interconnected by gap junctions (legend continues next page).

(B) The model neurons display subthreshold membrane oscillations (STOs), represented by the lower circle, and spiking, represented by the upper circle. The colors indicate which current dominates which part of the activity pattern: Ih current (green), a hyperpolarization-activated cation current, underlies a rise in membrane potential. Subsequently the It current (red), mediated by low threshold T-type Ca2+ channels, further drives up the membrane potential and from here either the sub-threshold oscillation continues (lower circle) or a spike is generated (upper circle), mediated though INa and IK currents (yellow and blue, respectively). Both after a spike or a subthreshold peak, influx of Ca2+ will trigger the activation of the hyperpolarizing K+ current by Ca2+-dependent K+ channels (blue). This hyperpolarization will again activate the Ih current starting the oscillation cycle again. A resulting trace of the subthreshold membrane potential oscillation punctuated with one spike is shown on the right. (C) 3D connectivity scheme of the 200 neurons in the network model. Links indicate gap junctional interconnections; the color of each neuron in the model represents the number of neurons to which that cell is connected through gap junctions. The thick green lines indicate first and second order neighbors of the center cell as an example. (D-E) Membrane potential of cells in the absence of input, for networks with and without coupling. (F-G) Cell activity sorted by amplitude, indicating that coupling the networks bring many cells into oscillating. (H-I) Distribution of STO frequency and amplitude for coupled (with gap junctions) and uncoupled (without gap junctions) model networks.

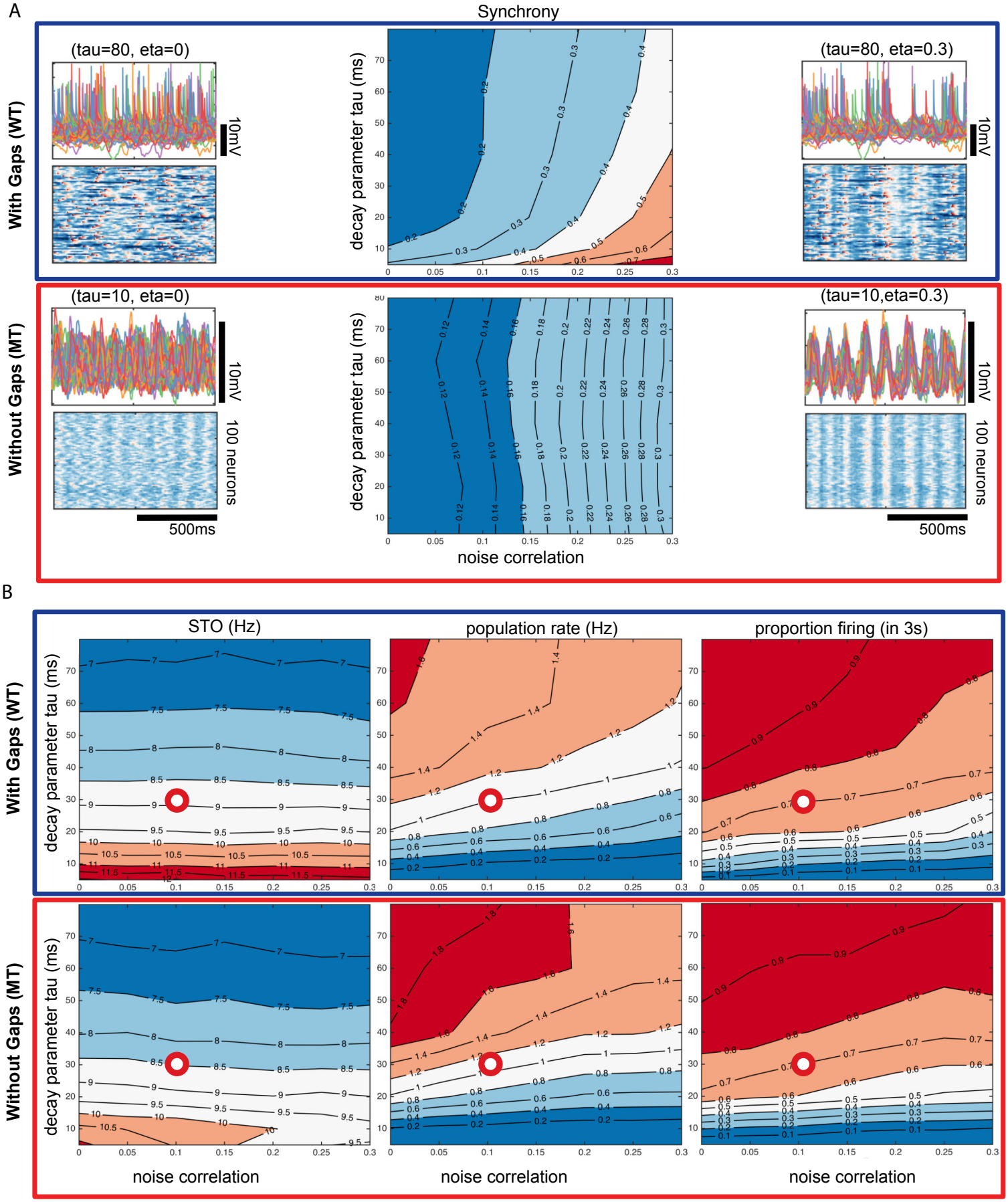

Fig. S4 - Behavior of model networks of identical cell composition as a function of the decay parameter of the Ornstein-Uhlenbeck process (tau) and the noise correlation (eta). Model networks have been computed using a systematic exploration of the parameter space using 56 instances of the network model. The contour plots indicate isolines for synchrony (A), frequency of subthreshold oscillations (STOs), population firing rate and proportion of active cells (B). The results presented in the main text come from a model network with parameters chosen such as to display STOs with mean of 9 Hz, a population rate of about 1 Hz and with more than 70% of cells firing in three seconds (95% of cells fire within 10 s of simulation time). The position of this network in the contour plots is indicated with a red circle. In A, the thumbnails exemplify behaviors of extreme instances of the model network both as membrane potentials traces (top) and as heatmaps of the membrane potential (bottom). Arrows indicate parameter space coordinates of these examples. The decay of the Ornstein-Uhlenbeck process (tau) mostly impacts the firing rate of the model networks, while noise correlation (eta) has a direct effect on synchrony. (B) Gap junctions amplify the input correlation given to the neurons, while having a minor effect on other aspects of the network dynamics.

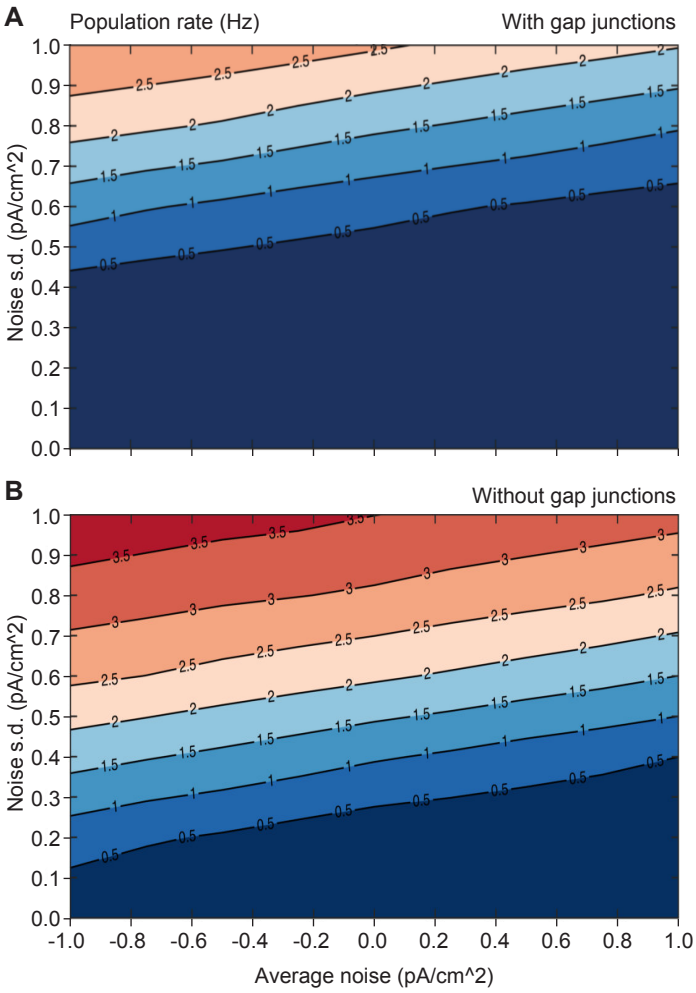

Fig. S5 - Contour plot indicating the average firing rate of networks as a function of the mean and standard deviation of the OU input. (A) Baseline input was chosen such that the cells of the model networks would produce approximately 1 Hz of spontaneous firing rate. The absence of gap junctional coupling in “mutant” model networks (B) leads to increased firing rate, which was compensated for by increasing the leak current of the membrane by 0.003 mS/cm^2.

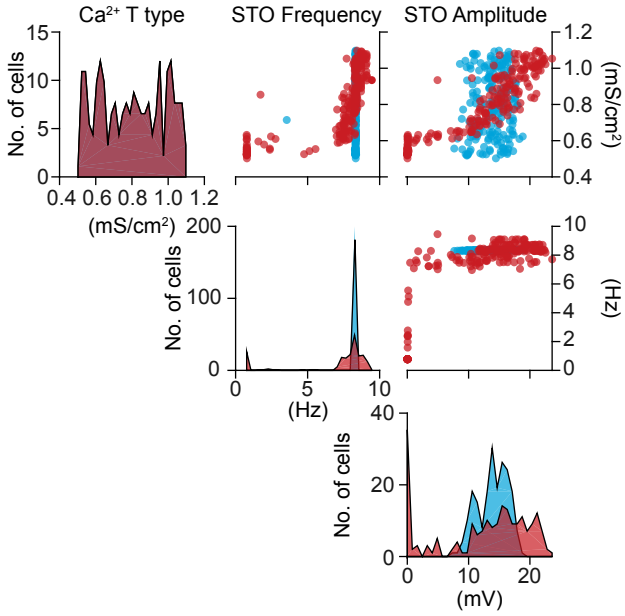

Fig. S5 - Physiological properties of the individual model cells as a function of Ca2+ T-Type conductance the absence of “contextual input” in the presence (blue) and absence (red) of gap junctional coupling. The Ca2+ T type conductance is varied in the range of 0.5 to 1.1 mS/cm2, resulting in a range of oscillatory properties of the individual model cells. The left axis in the panels of the main diagonal display cell counts for the histograms. The right axis besides the rightmost panel displays the indicated continuous variable. The set of non-oscillating (zero amplitude, zero frequency) cells constituted about 25% of the model network in the absence of gap junctions (red), were engaged in the oscillation when gaps were added to these cells (blue). In the absence of “contextual input” the distribution of frequencies had peaks at zero and sharply synchronizes at approximately in the absence of Ornstein-Uhlenbeck input.

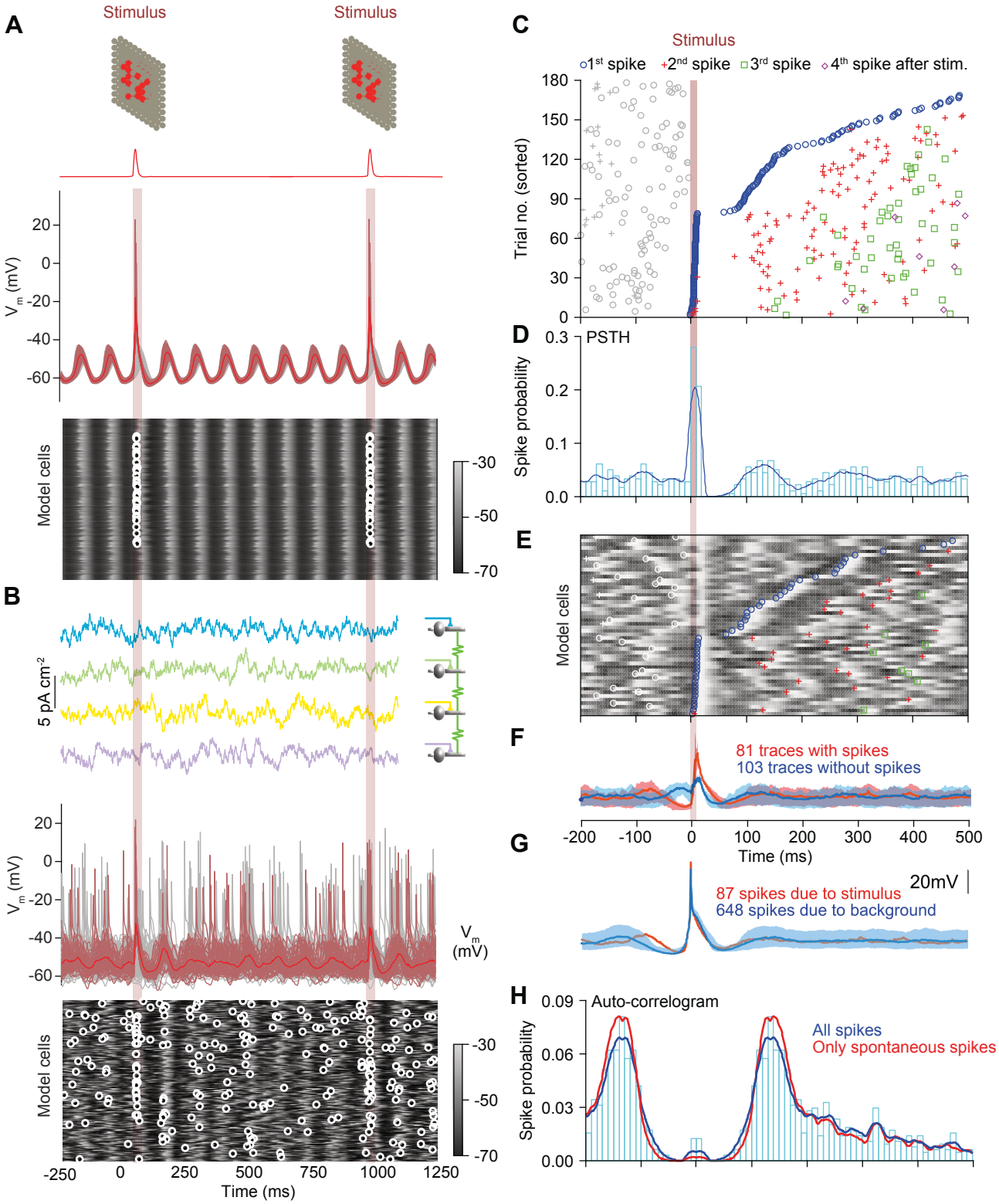

Fig. 10. Synaptic input strongly affects the oscillatory behavior in a network model of the inferior olive. (A) A phasic and synchronous input mimicking sensory input (see Fig. 9A) was delivered to a subset of cells (indicated in red) of the model network. Membrane potentials of all 200 cells in the model network in the absence of "contextual input" (see Fig. 9A). Pink traces represent the membrane potentials of cells directly stimulated by the "sensory input" (see A), with the red trace being their average. Below are the membrane potentials of the model cells as a heat map. Each row represents one model cell and the small circles indicate the occurrence of spikes. In the absence of "contextual input", model neurons displayed long lived and regular transient subthreshold oscillations following each "sensory input". These patterns changed dramatically, however, after adding "contextual input". This "contextual input" models the combination of inhibitory and excitatory inputs from other brain regions to the inferior olive.

(B). While in the absence of “contextual input”, model neurons showed synchronous subthreshold oscillations and were silent except upon receiving “sensory input”, now – in the presence of “contextual input” – spikes occur throughout the simulation and the subthreshold oscillations are unstable and not synchronized. Note that despite the largely uncorrelated “contextual input”, model cells did not fire homogenously, but loose clusters were present. (C) Rhythmic responses to stimulation are reproduced by the inferior olivary network model. From the model network, we present a cell with responses to “sensory input” that reproduce oscillatory features of the PSTH and autocorrelogram as found in vivo (see Fig. 2). Raster plot of olivary spiking triggered by 182 stimuli (“sensory input”), ordered by latency to the first spike following the stimulus. As seen in the in vivo data, the first spike after the stimulus can fall in multiple windows of opportunity. For this simulation, we included the “contextual input”. (D) Peri-stimulus time histogram showing the response peaks upon “sensory input”. (E) Autocorrelograms comparing spikes produced during stimulation with spikes due to background (spontaneous) activity. Periodic stimulus delivered to the network reduced resonant response at the peak. The extreme short-latency responses (in the center of the autocorrelogram) are due to spikelets that can also be seen in C. (F) Raster plot like in C, but with overlaying membrane potentials. For clarity, only the first 50 stimuli are displayed. Spike symbols follow conventions in C. Trials with low latency were preceded by a dip in the preceding membrane potential, a phenomenon that can also be clearly observed in G and H. (G) Average membrane potential of this neuron aligned by spikes that were either due to “sensory input” (19 spikes; red) or produced spontaneously (61 spikes; blue). The light shaded backgrounds represent the 10% and 90% percentile ranges of membrane potential. Dips in membrane potentials preceding spike reveal that for both groups a prior inhibition increased the probability of spiking. Importantly except for a refractory period, we did not observe a clear oscillation pattern following either spike type, due to variability imposed by the “contextual input”. (H) Average membrane potential traces of this neuron aligned to stimulus, separating trials with from trials without a spike. Clearly, stimulus-evoked spikes were most likely related to preceding dips in the membrane potential.

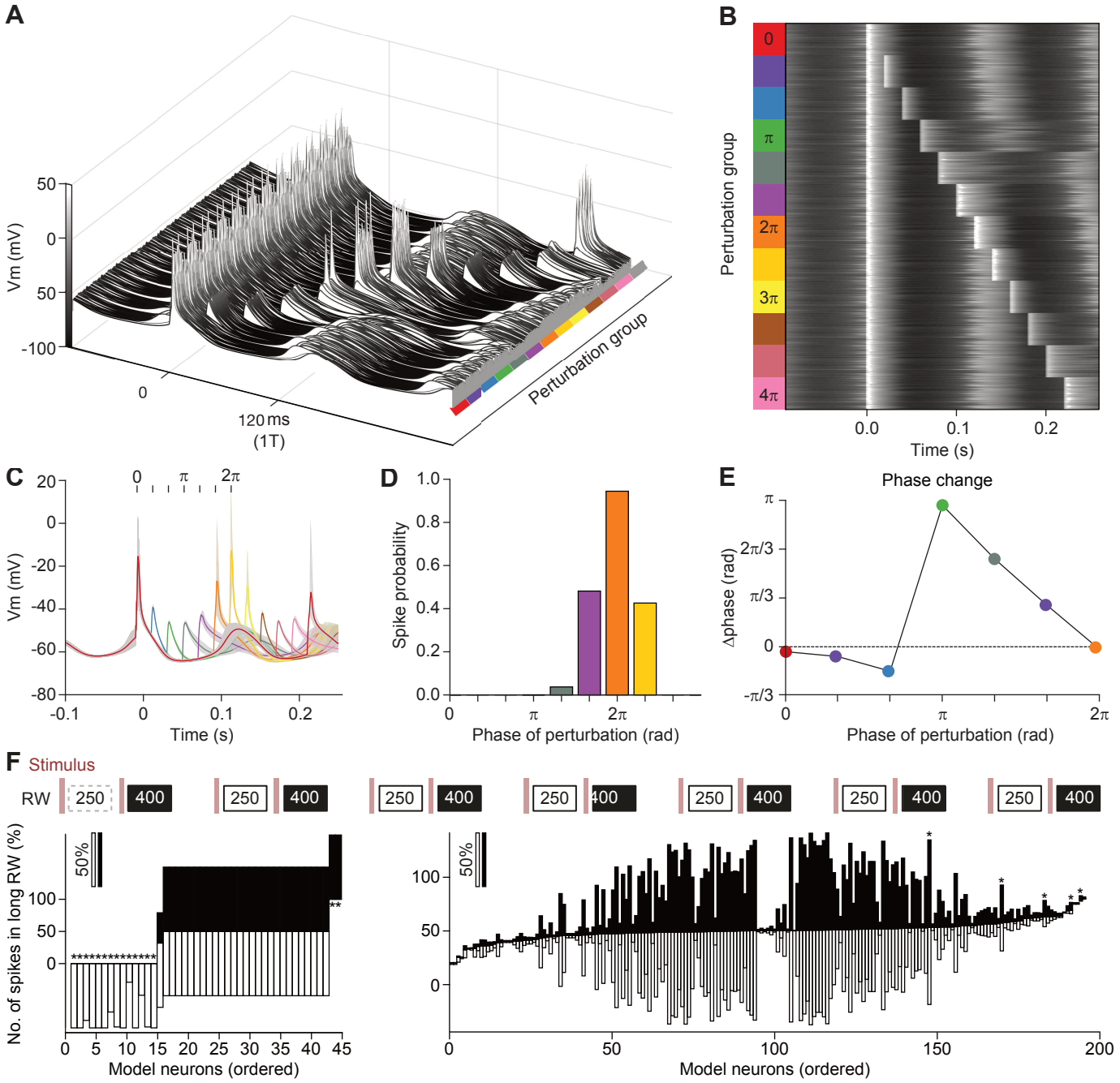

Fig. 11 Synaptic input determines the phase-dependent gating properties of the inferior olive network model. (A) Phase-dependent spiking was very prominent in our network model of the inferior olive in the absence of "contextual input". We repeatedly stimulated the same 54 model cells with synchronous "sensory input" (cf. Fig. 9A). The other 146 neurons of the network model were present, but not stimulated. The phase-dependent gating was studied using tandem stimulation with varying inter-stimulus intervals. The membrane potential of each of these 54 model neurons is plotted in A as a waterfall plot and in B as a heat map. The simulations are grouped by the interval between the two stimuli, starting with a single stimulation (bottom, red), and continuing with small to large intervals. In 13 equal steps two whole cycles of the subthreshold oscillation were covered. (C) Average and inter-quartile range (shaded area) of membrane potentials of neurons in the network that were only perturbed once at 0 ms ("red perturbation group" in A and B). The phase of the subthreshold osillations of the "synchronized" cells in the network was used to compute the data displayed in D and E. (D) Spike probability plot as measured for the second perturbation at the different phases of the membrane oscillation. Spike probability was computed as the number of neurons firing divided over the total number of neurons getting input. The first perturbation given at the peak of the oscillation is demarked as the start of the oscillation cycle. We see that secondary perturbations at both a half and one-and-a half cycle (?) and 3?, respectively) did not trigger spikes, while perturbations following at either one or two full oscillation cycles (2? and 4?, respectively) did trigger spikes. The repetition of the 'sinusoidal' probability curve shows that the spiking impediment is not (only) due to a refractory period, but follows the phase of the oscillation, being in more hyperpolarized states (not shown). (E) Phase response curve showing that perturbations early in the oscillation phase did not impact much on the timing of the spike, but halfway the oscillation the perturbations advanced the ongoing phase considerably which declined linearly to the end of the full cycle. The average membrane potential at the perturbation at 0 ms only went up to -15 mV and not up to the average spike height of approximately 10 mV, because in the population making up the average not all neurons spiked. (G) In order to test the impact of the presumed phase of the inferior olivary neurons, we applied a "gallop" stimulation pattern, alternating short (250 ms) and long (400 ms) intervals. "Sensory input" (vertical grey bars) were delivered and complex spikes were counted in response windows (RW) 0-180 ms post-stimulus. Response probabilities were compared between RWs in short and long intervals. The first response window is not included in the analysis because it is not preceded by a stimulus interval.

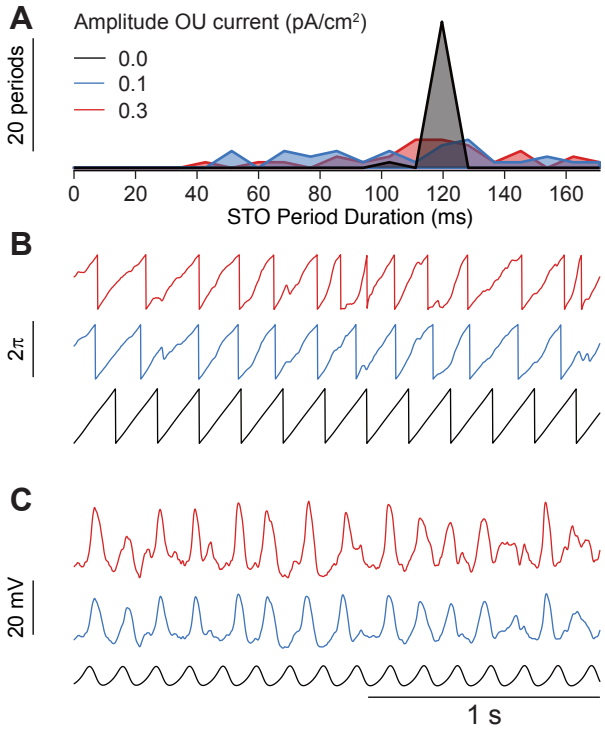

Fig. 12. Significant variability of oscillatory periods induced by contextual input on oscillation period of a single model cell. (A) Distribution of inter-peak intervals for a single model cell under 5 s of contextual stimulus of different amplitudes. To gauge period variability without introducing refractory periods, input levels were chosen for non-spiking subthreshold dynamics only. The unperturbed model cell (in black) produces regular periods, while weak contextual stimulus is sufficient to create substantial variability (red and blue). (B) Example traces of membrane potential and (C) phase for the single cell under perturbations, for the same random seed. Note that under contextual input there was substantial variation in periods, but similar STO periodicity despite different levels of input.

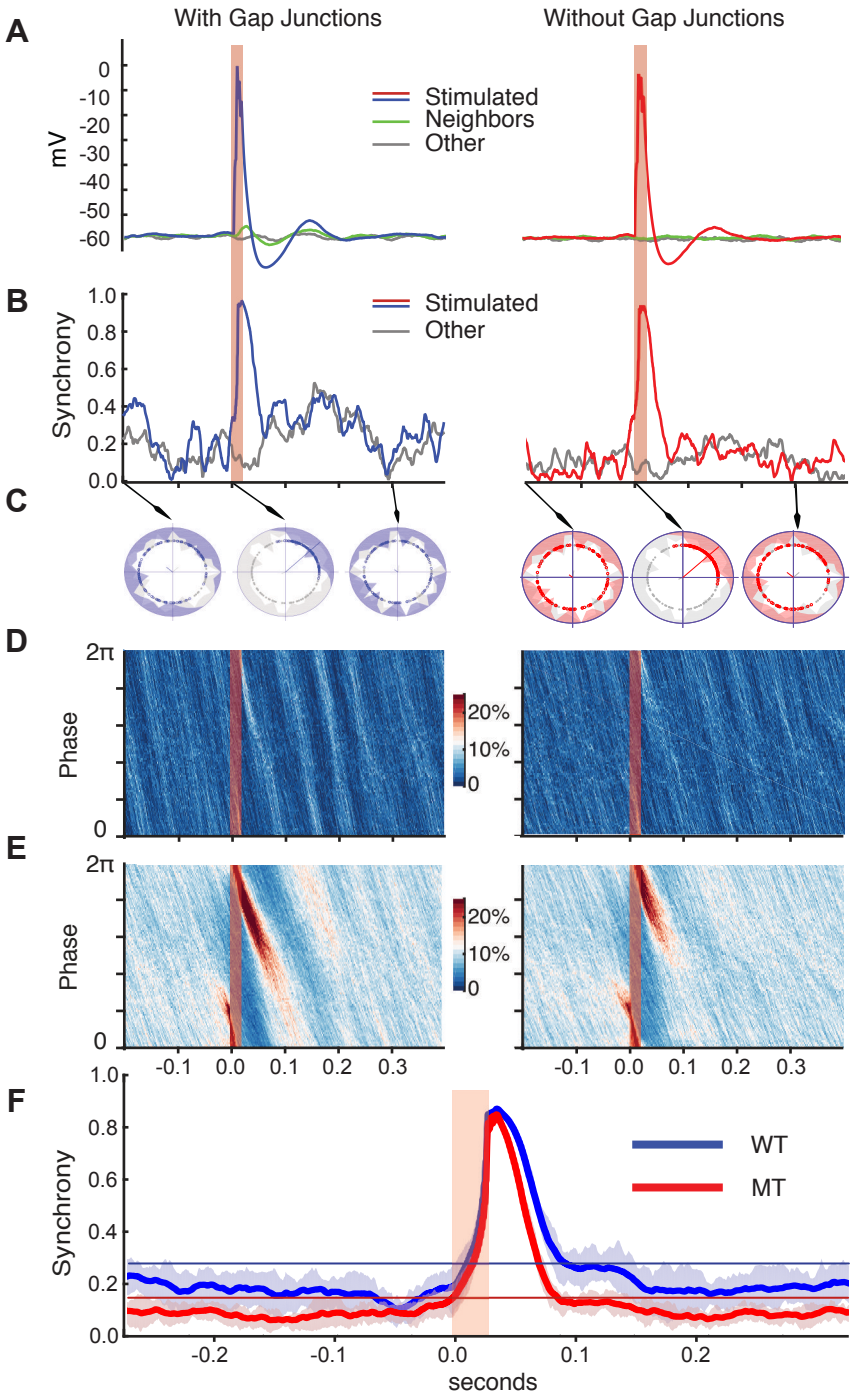

Fig. 13. Impact of periodic stimulation on network phase in the presence of contextual stimuli for networks with (left column) and without gap junctions (right column). Gray bars indicate stimulation time. (A) Stimulus triggered membrane potential for all cells in the network (N=100 stimuli). Stimulation causes a peak in the membrane potential of the directly stimulated cells (mask). The effect of the current spreading through gap junctions is visible in the cells immediately neighboring the stimulated cells (green line), while it was absent in the network model without gap junctions. (cont. next page)

(B) Increase of synchrony in the network due to a single stimulus. Synchrony is displayed as phase concentration over time (the Kuramoto parameter) for cells under the stimulation mask (colored) and other cells (gray). Stimulation generated a transient synchrony peak in both networks but is considerably higher and longer lived in cells with gap junctions, due to synchrony inducing current flows. (C) Polar plots indicating network phase distribution for snapshots (arrows) for stimulated (colored distribution) and non-stimulated cells (gray distribution). Phase alignment of subthreshold oscillations of the inferior olivary network model was reduced in the absence of gap junctions. (D) Phase distribution of cells over time. Color code represents the proportion of neurons occupying a certain phase at a given time (phase bin size is 2pi/100, time bin is 1 ms). Dark/Light bands indicate that the phase alignment propagates to most cells in the network and subsists for longer durations for the WT network. Nevertheless, “contextual input” overruled the phase alignment within a few hundred milliseconds (~300 ms in this case). In the absence of gap junctions, the impact of the stimulus is restricted to stimulated cells, so that the coherence induced by stimulus on the network was much smaller. (E) Same as D but displaying averaged phase distributions from 100 stimuli. After 200 ms the effect of the stimulus was hardly noticeable, and there was no indication of entrainment, which would be visible as vertical bands before the stimulus. This is because the effect of the stimulus is not stereotypical, due to dependency on network state and contextual input (see also Fig. 11). (F) Average network synchrony triggered on the stimulus. The horizontal lines in the bottom plot are the 95% inclusion boundaries taken from the 5 s of spontaneous network behavior to contextual input (no periodic “sensory” pulses). The model network with gap junctions displayed an elevated synchrony plateau after the stimulus, which ended after around about 200ms, disappearing visibly earlier in the absence of gap junctions. There was no preceding synchrony, indicating complete absence of entrainment to the periodic stimulus.